Arteriosclerosis, Thrombosis, and Vascular Bi

BASIC SCIENCES

Deficiency of *ZC3HC1* Modulates Vascular Smooth Muscle Cell Phenotype and Increases Neointima Formation

Redouane Aherrahrou,* Tobias Reinberger,* Julia Werner, Miriam Otto, Jaafar Al-Hasani, Maria Loreto Munoz-Venegas, Xiaoke Yin, Manuel Mayr, Mete Civelek, Heribert Schunkert, Thorsten Kessler, Zouhair Aherrahrou

BACKGROUND: The *ZC3HC1* (zinc finger C3HC-type containing 1) gene has been linked to various cardiovascular traits, including coronary artery disease, blood pressure, and carotid intima-media thickness with opposing effects. This study aimed to investigate the role of ZC3HC1 in smooth muscle cell (SMC) biology and its contribution to neointima formation.

METHODS: SMC phenotypes (proliferation and migration) were analyzed according to rs11556924 genotype, small interfering RNA–mediated knockdown of human ZC3HC1, or complete knockout of murine Zc3hc1. Transcriptomic profiling and contractile marker expression were used to define SMC states. The impact of complete gene loss on injury-induced neointima formation was examined in vivo using Zc3hc1$^{-/-}$ mice. Subcellular localization of murine NIPA (nuclear interaction partner of anaplastic lymphoma kinase; encoded by Zc3hc1) during the cell cycle was analyzed by immunofluorescence microscopy.

RESULTS: The coronary artery disease–protective rs11556924-T allele was associated with reduced *ZC3HC1* expression and enhanced SMC migration. *ZC3HC1* knockdown in human SMCs replicated this phenotype, increasing migration and proliferation, and leading to CCNB1 (cyclin B1) accumulation with reduced expression of contractile markers. Following arterial injury, *Zc3hc1*$^{-/-}$ mice exhibited exaggerated neointima formation and enhanced SMC migration. In contrast to small interfering RNA experiments, complete *Zc3hc1* loss resulted in reduced SMC proliferation and lower CCNB1 levels. Transient knockdown of *Zc3hc1* in wild-type mouse SMCs increased proliferation, recapitulating findings in human cells. Immunofluorescence revealed colocalization of NIPA and CCNB1 at the cleavage furrow, suggesting a role in mitotic exit.

CONCLUSIONS: ZC3HC1 acts as a dosage-sensitive modulator of SMC phenotype. Partial reduction promotes a synthetic, proliferative state and neointima formation, while complete loss induces a quiescent phenotype. These findings provide mechanistic insight into the paradoxical clinical associations of the rs11556924-T allele and identify ZC3HC1 as a potential target for modulating SMC phenotypes in vascular disease.

GRAPHIC ABSTRACT: A graphic abstract is available for this article.

Key Words: coronary artery disease ■ cyclin B1 ■ drug-eluting stents ■ muscle, smooth, vascular ■ neointima

Coronary artery disease (CAD) caused by atherosclerosis is the leading cause of death in the developed world.[1] Due to atherosclerotic deposits, the lumen of the vessels becomes narrow, limiting the supply of oxygen-rich blood to the affected tissue. This reduction in blood flow may result clinically in the development of chest pain and, in the event of atherothrombosis, in myocardial infarction. Implantation of coronary stents is the primary therapeutic option to reopen an occluded coronary artery in patients after myocardial infarction. Despite the development of drug-eluting stents and balloons, restenosis due to neointima formation remains a major limitation after coronary intervention.

Genome-wide association studies have identified the single-nucleotide polymorphism rs11556924 at the

Correspondence to: Zouhair Aherrahrou, PhD, Institute for Cardiogenetics, Universität zu Lübeck, Ratzeburger Allee 160, 23562 Lübeck, Germany. Email zouhair.aherrahrou@uni-luebeck.de
*R. Aherrahrou and T. Reinberger contributed equally.
Supplemental Material is available at https://www.ahajournals.org/doi/suppl/10.1161/ATVBAHA.125.323659.

Arterioscler Thromb Vasc Biol is available at www.ahajournals.org/journal/atvb

Nonstandard Abbreviations and Acronyms

ACTA2	smooth muscle actin alpha 2
APC/C	anaphase-promoting complex/cyclosome
CAD	coronary artery disease
CCNB1	cyclin B1
CNN1	calponin 1
ECM	extracellular matrix
FBS	fetal bovine serum
IMT	intima-media thickness
LMOD1	leiomodin 1
NIPA	nuclear interaction partner of anaplastic lymphoma kinase
PDGF	platelet-derived growth factor
RNAseq	RNA sequencing
SCF	Skp, Cullin, F-box containing complex
siRNA	small interfering RNA
SMC	smooth muscle cell
SmGM-2	smooth muscle medium-2
SRF	serum response factor
TPR	translocated promoter region, nuclear basket protein
WT	wild type
ZC3HC1	zinc finger C3HC-type containing 1
α-SMA	alpha smooth muscle actin

What Are the Clinical Implications?

Genetic variation at the *ZC3HC1* locus has been associated with coronary artery disease, blood pressure, and carotid intima-media thickness, yet the underlying vascular mechanisms have remained unclear. Our study functionally identifies *ZC3HC1*/NIPA (nuclear interaction partner of anaplastic lymphoma kinase) as a regulator of vascular smooth muscle cell phenotype and neointima formation, linking human genetic risk to cellular and vascular remodeling processes. Our findings suggest that partial loss of *ZC3HC1* promotes a migratory, synthetic smooth muscle cell phenotype that may accelerate early lesion development and restenosis, whereas complete loss suppresses proliferation and alters vascular repair dynamics. These results offer mechanistic insight into previously reported genetic associations in patients and highlight the importance of disease stage when interpreting smooth muscle cell phenotype. Clinically, this work supports strategies that specifically target smooth muscle cell phenotypes, rather than broadly inhibiting proliferation, as a more nuanced approach to preventing restenosis and modulating atherosclerosis progression.

chromosome 7q32.2 CAD susceptibility locus, which harbors the *ZC3HC1* (zinc finger C3HC-type containing 1) gene (HUGO Gene Nomenclature Committee: 29913).[2–8] *ZC3HC1* encodes the nuclear-derived protein, NIPA (nuclear interaction partner of anaplastic lymphoma kinase),[9] an essential component of the SCF (Skp, Cullin, F-box containing complex)–type E3 ubiquitin ligase complex that initiates the degradation of CCNB1 (cyclin B1).[7,10] The CAD-associated variant rs11556924-T is a nonsynonymous variant, leading to an amino acid substitution p.Arg363His in the canonical transcript of *ZC3HC1* and ≈4.9% to 7.0% reduction in CAD risk per allele.[4,6,11,12] The CAD risk variant rs11556924-C (Arg363) is associated with lower phosphorylation of NIPA, resulting in increased NIPA activity. This hyperactive NIPA accelerates CCNB1 degradation, thereby slowing nuclear CCNB1 accumulation and prolonging mitosis. Altered cell-cycle regulation may impair normal repopulation and repair processes in vascular tissue, possibly contributing to CAD pathology.[7] However, the same genetic variant increases the risk of carotid intima-media thickness (IMT) in patients with rheumatoid arthritis.[13]

Because CCNB1 and cyclin-dependent kinase form the M phase–promoting factor, NIPA is involved in regulating the cell cycle at the G2 to M phase transition.[10] In addition, the zinc finger protein NIPA has been recently referred to as a genuine nuclear basket protein of 53 to 55 kDa in vertebrates (≈84% similarity to the murine ortholog[14]), residing in the nuclear envelope and interacting with the nucleoprotein TPR (translocated promoter region, nuclear basket protein)[15] that is involved in messenger RNA export, chromatin compartmentalization in the interphase, and mitotic spindle checkpoint signaling during mitosis.[16]

To understand the link between NIPA modulation and vascular remodeling, we assessed the role of *ZC3HC1* in human and murine vascular smooth muscle cells (SMCs), a key cell type involved in neointima formation following injury.[17] Specifically, we analyzed the effects of *ZC3HC1* modulation on migration and proliferation of primary human and mouse aortic SMCs in vitro. Subsequently, we used wire injury to induce neointimal hyperplasia[18] in vivo in *Zc3hc1*-deficient mice. Our findings showed that *ZC3HC1* deficiency was accompanied by CCNB1 alteration, increased migration, modified proliferation rates of vascular SMCs, and enhanced neointima formation in mice. For clarity, the name *ZC3HC1/Zc3hc1* is used to describe the gene, and hNIPA (human NIPA protein) or mNIPA (mouse NIPA protein) to refer to the human or murine protein.

MATERIALS AND METHODS

The data that support the findings of this study are available from the corresponding author upon reasonable request. Tables S1 through S9, Uncropped Western Blots, and the Major Resources Table are available in the Supplemental Material.

A subset of Python scripts can be found at GitHub (https://github.com/ToReinberger/ZC3HC1_in_SMCs).

Expression Quantitative Trait Locus Analysis of ZC3HC1 in Human SMCs

Primary human aortic SMCs were isolated from the ascending aortas of 151 heart transplant donors (both male and female) at the University of California, Los Angeles, or obtained from commercial suppliers (Lonza and PromoCell), as this has been previously described.[19] The University of Virginia institutional review board has ruled that specimens used for cell collection do not fall under the purview of current regulations governing the participation of human subjects in research because these specimens have no identifying information. All SMCs were maintained in SMC basal medium (CC-3181, Lonza) supplemented with SmGM-2 (smooth muscle medium-2, CC-4149, Lonza). Briefly, the stranded libraries of high-quality ribosomal RNA-depleted total RNA were sequenced to ≈100 million read depth with 150-bp paired-end reads at the Psomagen sequencing facility. The reads with average Phred scores <20 were trimmed using Trim Galore, followed by mapping the reads to the hg38 (human genome reference assembly GRCh38) version of the human reference genome using the STAR Aligner[20] in 2-pass mode. Gene expression of *ZC3HC1* was quantified by calculating the number of transcripts per million using RNA-SeQC.[21] Expression quantitative traits locus analysis was performed using tensorQTL[22] after correcting for sex, genotype PCs, and hidden confounding variables.

Quantification of Migration in 151 Primary SMCs

Migration was monitored continuously every 15 minutes for 24 hours using electronically integrated 16-well Boyden chamber plates (CIM-plate 16; ACEA Biosciences), which feature 8-µm pores. This was conducted with the xCelligence Real-Time Cell Analysis Instrument (ACEA Biosciences, Inc, San Diego, CA) situated in a 5% CO_2 humidified incubator maintained at 37 °C. Thirty thousand cells were seeded into the upper chamber of each well using serum-free media. The lower chamber contained either serum-free media as a control or serum-free media supplemented with 100-ng/mL PDGF (platelet-derived growth factor)-BB as a chemoattractant. The instrument monitored changes in electrical impedance as the cells migrated to the lower chamber, translating these changes into an index that was proportional to the number of migrating cells. All experiments were conducted in quadruplicate for each condition. Data were analyzed using RTCA software, version 1.2 (ACEA Biosciences, Inc), combined with R software. The migration rate is displayed as the normalized Log10 of time needed to reach saturation in the xCELLigence Biosensor buildup curve. The association between the genotype of rs11556924 and migration was calculated using a linear mixed model to account for multiethnic population composition, as previously described.[19]

Silencing of ZC3HC1 Gene Expression Using Small Interfering RNA

The experiments were conducted at the University of Lübeck, Germany, where the infrastructure was optimized for small interfering RNA (siRNA)–based gene silencing. Dicer siRNA targeting the *ZC3HC1* gene (*ZC3HC1* siRNA, Integrated DNA Technologies-ID: hs.Ri.ZC3HC1.13.2) and scramble control siRNA were purchased from Integrated DNA Technologies. Human aortic SMCs (Cell Applications, Inc, 354-05a, C/C genotype for rs11556924) in M231 cell culture medium (Gibco) with smooth muscle growth supplement (Gibco) were cultured in 48-well cell culture plates (Greiner Bio-One) at a density of 0.4×10^5 cells per well for 24 hours. The cells were transfected with 5- to 30-nmol/L *ZC3HC1* siRNA or 5- to 30-nmol/L control siRNA overnight using GenMute SMC siRNA Transfection Reagent (SignaGen Laboratories) according to the manufacturer's instructions. The transfected cells were subsequently incubated in M231 smooth muscle growth supplement culture medium for 48 hours, after which the samples were harvested and stored at −80 °C until used for quantitative polymerase chain reaction and Western blot analyses.

Cell Migration and Proliferation of ZC3HC1-Knockdown SMCs

To determine the role of *ZC3HC1* gene expression knockdown in SMC migration, wound-healing assays with ibidi 4-well culture inserts in a 12-well plate format were performed at the University of Lübeck, as described.[23] Briefly, ≈2.2×10^4 SMCs (Cell Applications, Inc, 354-05a, C/C genotype for rs11556924) per well were seeded into insert wells and incubated at 37 °C and 5% CO_2 for 24 hours. Following siRNA transfection overnight (see above), the cells were incubated in M231 culture medium supplemented with smooth muscle differentiation supplement (Gibco), which contains only 1% (v/v) fetal bovine serum (FBS) and 30-µg/mL heparin. After 48 hours, the inserts were removed, and the cells were washed with PBS and cultured in M231 smooth muscle differentiation supplement medium supplemented with 5-ng/mL PDGF-BB (PeproTech) to provoke cell migration. Images taken at 0 and 12 hours with an Olympus IX70 microscope were analyzed using an in-house Python script. In brief, images were converted into binary matrices and processed using the methods GaussianBlur and adaptiveThreshold in the OpenCV package cv2. To calculate the migration distance in a binary matrix with x-y dimensions, the left and right cell layer edge (ie, start-x_y and end-x_y position) is first identified in the 0-hour image for each y-slice (ranging from 0 to image height). Next, the sum of positive pixels within the growth area (from start-x_y to end-x_y) is calculated for each y-slice. Finally, the average of these sums across all y-slices serves as an indirect measure of cell migration. Experiments were performed in triplicate; 2 ibidi 4-well culture inserts were used for each replicate and condition, resulting in 2 means of 4 values per replicate. To assess the proliferation of *ZC3HC1* knockdown SMCs, the cells were plated into 96-well plates (0.6×10^4 cells/well) and transfected as described above. The next day, the cell culture medium was replaced with M231 medium supplemented with 1% FBS to starve the cells. These human SMCs were subsequently treated with 100-ng/mL PDGF-BB (PeproTech) to induce proliferation. To quantify the proliferation rate, the cell nuclei were stained with Hoechst 33342 dye (Thermo Fisher Scientific) at several time points, and the number was counted using an in-house Python script, CellCounter.py. Six wells were analyzed per condition, with all experiments performed in triplicate. The

values were normalized to time point 0 to account for small differences in initial cell numbers after siRNA transfection. To confirm the proliferation results, a bromodeoxyuridine-based proliferation assay was conducted according to the manufacturer's instructions (Roche, 11647229001). The incorporation of bromodeoxyuridine was detected colorimetrically after 6 to 8 hours of incubation time at a wavelength of 370 nm and normalized to cells devoid of bromodeoxyuridine. In addition, cell nuclei were stained with Hoechst 33342 dye. Proliferation assays were performed in 3 and 5 replicates, respectively.

Quantitative Polymerase Chain Reaction Analysis

These analyses were performed as described.[21,22] Briefly, total RNA was isolated from cultured cells using RNeasy plus kits (Qiagen, Valencia, CA) and reverse transcribed into cDNA. Messenger RNA levels were determined by relative quantitative RT-polymerase chain reaction and analyzed using the ΔΔCT method relative to the internal standard, GAPDH/Gapdh.[24] The primers (Eurofins Genomics) used in this study are shown in the Supplemental Material.

Western Blot Analysis

Western blot analyses were performed as previously described.[25] Briefly, 15- to 75-µg samples of protein isolated from cultured cells were electrophoresed on SDS-PAGE gels and transblotted onto nitrocellulose membranes. The blots were treated with 5% skim milk and incubated with primary antibodies, including anti-NIPA (phospho S354) antibody (Abcam ab63557, 1:500), anti-CCNB1 antibody (Abcam ab181593, 1:300), anti-SRF (serum response factor; Cell Signaling Technology, SRF [D71A9] XP, 1:500), anti-CNN1 (calponin 1; Abcam ab46794, 1:500), anti-LMOD1 (leiomodin 1; Proteintech 15117-1-AP, 1:500), and anti-GAPDH antibody (loading control; Abcam ab181602, 1:2000). Amido black dye (Sigma-Aldrich A8181-1EA) served as internal loading control. The blots were subsequently incubated with the appropriate secondary antibodies. Protein bands were detected using the ECL Prime Western blotting Detection Reagent (GE Health Care) and quantified using ImageJ software.

RNA Sequencing

Human aortic SMCs (Cell Applications, Inc, 354-05a) were seeded into 6-well plates at a density of 3.1×10^4 cells/cm^2 and transfected with siRNA as described above. After 2 days in M231 smooth muscle differentiation supplement medium, 5-ng/mL PDGF-BB (PeproTech) was added. Cells devoid of PDGF-BB served as an internal control. After incubation for 24 hours, the RNA was extracted using innuPREP RNA Mini Kits 2.0 (Analytik Jena), yielding ≈5-µg total RNA (RNA integrity number >7) per sample. RNA sequencing (RNAseq), including ribosomal RNA-depletion and quality control, was performed at the Novogene sequencing facility (NovaSeq 6000 PE150, 150-bp paired-end reads). After trimming reads with low average Phred scores (<20) using Trim Galore, all included samples passed the quality control analysis. Reads were mapped to the hg38 version of the human reference genome using the STAR Aligner[20] in 2-pass mode, with gene expression quantified by calculating transcripts per million using RNA-SeQC.[21]

Differential Gene Expression and Functional Enrichment Analysis

A total of 17 242 genes with >6 reads were included in at least 20% of the samples in at least 1 of the 2 conditions (ZC3CH1 siRNA and control siRNA) for differential expression analysis using DESeq2, controlling for batch effect.[26] Genes were considered to be differentially expressed under treated and untreated conditions when P_{adj} was <0.05 and $\log_2$(fold change) was >0.4. Principal component analysis was performed using R. PDGF-BB treatment was defined as a covariate. Network analysis and Gene Ontology enrichment after clustering were performed to characterize the functional consequences of differences in gene expression associated with downregulation and normal expression of *ZC3HC1*.[27] In brief, a functional gene network containing differentially expressed genes (P_{adj}<0.05) was constructed with the help of the STRING (Search Tool for the Retrieval of Interacting Genes/Proteins) database repository (https://string-db.org/) using the REST API implemented in Python. The following parameters were used: species: 9606, network_type: functional, network_flavor: confidence, score>0.4, and add_white_nodes: 30 for the complete gene network and 8 for the CCNB1 subnetwork. Agglomerative ward clustering of the gene network was performed using the scikit-learn (version 0.24.2) clustering package. Gene set enrichment of each cluster was performed using the REST API of STRING.[27] Gene networks were visualized by the Python packages networkx (version 4.4.0) and matplotlib (version 40.8.0).

Proteomics

The proteomic analysis was conducted as described.[28] Primary SMCs from heart transplant donors carrying the T allele (n=7) or C allele (n=6) were cultured as described above. For both SMC types (knockdown/control and heart transplants), cells were washed 3× with cold PBS thoroughly, detached, and collected using centrifugation. After the addition of cell lysis buffer (9803, Cell Signaling), including protease inhibitors/phosphatase inhibitors (04906837001, ROCHE diagnostics/11697498001, ROCHE diagnostics), cells were sonicated on ice 2× for 15 seconds and left on ice for 20 minutes. The supernatant was subjected to mass spectrometry.[28] Normalized abundance values were kept if at least 2 unique peptides per protein were detectable, and >30% of samples exhibited mass spectrometry signals for the corresponding protein. In a pairwise comparison, missing values were replaced with 0 if >90% of replicates of group A showed signals and <10% of replicates of group B lacked mass spectrometry signals. After log2 transformation, missing values were imputed using k-nearest neighbors imputation, and differential protein levels were assessed with the aid of the limma R package,[29] adjusting for multiple testing using the Benjamini-Hochberg method.

Generation and Housing of Animals

Heterozygous *Zc3hc1* (±) mice (Zc3hc1tm1a[KOMP]Wtsi, background: C57BL/6 N) were obtained from KOMP (Knockout Mouse Project) at the University of California, Davis, California. They were created using a targeting construct of the mouse *Zc3hc1* gene, designed by introducing the EN2 splicing acceptor followed by the beta-galactosidase sequence

and a neomycin selection cassette 3' at exon 4. Heterozygous mice were initially backcrossed to a C57BL/6J genetic background for at least 6 generations and then used in Het×Het mating to generate sufficient numbers of *Zc3hc1* knockout ($^{-/-}$) and wild-type (WT or $^{+/+}$) littermates for the experiments. Homozygous *Zc3hc1* ($^{-/-}$) mice were found to be infertile. Mice were genotyped using polymerase chain reaction screenings of DNA samples isolated from ear biopsies. Mice were genotyped using the primers 5'-TTGACTGACAGAGGATGAGAGC-3' (forward) and 5'-GGGCCTTTAATCCCAACACT-3' (reverse), targeting the second *LoxP* site located between exons 5 and 6 in the *Zc3hc1* gene. The expected lengths of the DNA fragments were 298 bp for the knockout and 260 bp for the WT mice (Figure 4A, right). In addition, β-gal-activity was measured in heart cryosections from one mouse per genotype (*Zc3hc1* $^{+/+}$, or $^{-/-}$) as described.[30]

Neointima Formation Mouse Model

All animal experiments were locally approved by the German animal studies committee of Upper Bavaria and conformed to the guidelines from Directive 2010/63/EU of the European Parliament on the protection of animals used for scientific purposes. Wire injury was induced in 8- to 12-week-old female mice as described[31] and established successfully in our group.[32] Female mice were selected to reduce sex-related variability in vascular injury responses because testosterone-driven differences in inflammation and smooth muscle remodeling can significantly affect neointima formation. The use of only female mice is consistent with established wire-injury protocols and supports the reduction of animal numbers in accordance with the 3R principles.

Briefly, all surgical procedures were performed under general anesthesia. Anesthesia was achieved by intraperitoneal injection of midazolam (5.0 mg/kg), medetomidine (0.5 mg/kg), and fentanyl (0.05 mg/kg; MMF [midazolam, medetomidine and fentanyl]) in 300 μL of 0.9% (w/v) sodium chloride. One-third of the dosage of MMF was added if the intertoe reflex was reestablished or the duration of anesthesia exceeded 60 minutes. After a skin incision, the left femoral artery was exposed by blunt dissection, and an angioplasty guidewire (0.015 inches in diameter, No. C-SF-15-15, COOK, Bloomington, IN) was introduced into the arterial lumen and inserted toward the iliac artery via arteriotomy. The wire was left in place for 1 minute to denude and dilate the femoral artery. After that, the wire was removed, and the blood flow of the femoral artery was restored. The arteriotomy site was ligated, and the skin was closed. The antagonists atipamezole (2.5 mg/kg), flumazenil (0.5 mg/kg), and naloxone (1.2 mg/kg) were administered subcutaneously to terminate anesthesia. Mice were euthanized 14 days later by intraperitoneal injection of pentobarbital. To remove blood inside the femoral arteries, the mice were perfused via the left ventricle and over the descending aorta with PBS (pH, 7.4). Femoral arteries were harvested and fixed in 4% buffered paraformaldehyde overnight.

Histology and Morphology

Paraffin-embedded femoral arteries were sectioned at 2-μm intervals and stained with hematoxylin and eosin. For morphometric analysis, images were digitized (Leica DFC450C camera), and serial sections in 50-μm intervals of each artery were blindly analyzed using ImageJ software (National Institutes of Health Image Software). Media area (M) and the area of neointima formation were quantified, and neointima-to-media ratios were calculated. Sections of paraffin-embedded femoral arteries were deparaffined through a series of decreasing concentrations of alcohol (3× xylol, 2×100% ethanol, 1×96% ethanol, 1×70% ethanol, and deionized water). For staining, slides were stained using hematoxylin and eosin solution (Carl Roth, T865.1). To fix the slides, they were treated with a series of increasing concentrations of alcohol (see above), followed by treatment with Cytoseal XYL (Thermo Fisher Scientific 8312-4). For immunohistochemistry staining, the slides were heated for 1.5 minutes in a microwave at 900 W and for 15 minutes at 90 W. For histochemistry, the slides were washed 3× with PBS, and unspecific binding was blocked by incubation with 5% (v/v) goat serum in PBS. Tissue slides were stained overnight at ambient temperature with anti-Ki-67 (1:100 in PBS, Thermo Fisher Scientific, Clone: B56, 15898578), anti-α-SMA (alpha smooth muscle actin/ACTA2 [smooth muscle actin alpha 2]; 1:100 in PBS, Abcam ab5694), anti-LMOD1 (1:200 in PBS Proteintech 151117-1-AP), or anti-CD31 (1:50 in PBS, Abcam ab28364) antibody, and primary antibodies were visualized using a horseradish peroxidase system (Santa Cruz, SC2004) and DAB (3,3′-diaminobenzidine) staining solution (DAKO, 3468). Cell nuclei were counterstained with hematoxylin. Slides were fixed with Aquatex (Merck 1085620050). To ensure consistency in our analysis, 5 sections within the injured area from each artery that exhibited the maximum neointima formation area were selected for quantification. Quantification of positively stained regions involved a 2-stage process combining manual segmentation of media and neointima with automated color-thresholding using a custom Python script.

Isolation and Culture of Murine SMCs

Mouse aortic SMCs were isolated from the thoracic aortas of WT and knockout (n=8–10) as reported previously.[25] Briefly, the thoracic aortas were collected, and fat and connective tissues were removed. The samples were predigested with collagenase II, and the adventitia was removed mechanically. Adventitia-free aortas were cut into small pieces and further digested with collagenase II with shaking for at least 6 hours, until complete tissue dissociation. The isolated cells were pelleted and resuspended in culture medium (DMEM plus 10% FBS and 1% penicillin/streptomycin, Gibco). Cells were expanded and grown on surfaces coated with 0.1% (w/v) gelatin. To quantify the purity of the populations, the isolated cells were characterized by flow cytometry using the SMC-specific fluorescein isothiocyanate-labeled anti-α-SMA antibody (Sigma, F3777) and an isotype control (mouse IgG2a-fluorescein isothiocyanate, Sigma F6522), yielding >95% purity.

Transient Knockdown of Zc3hc1 Gene Expression Using siRNA

Aortic SMCs isolated from the thoracic aorta of WT mice (background: C57BL/6J) were cultivated in DMEM (10% FBS, high-glucose, GLUTAMAX, and pyruvate) on flasks coated with 0.1% gelatin (Sigma G1890). Reverse transfection was performed in a 150-μL cell suspension mixed with 3.6-μL jetPRIME (Polyplus 101000046) and 4.95-μL DsiRNA (10 μM, mm.Ri.Zc3hc1.13.2). After 15- to 30-minute incubation at

room temperature, 1.5-mL DMEM with 3% FBS was added to the transfection mix, and 1.8×10^5 cells were seeded in gelatin-coated in each well of a 6-well plate (NUNC 140675). After 3.5 to 4 hours, the medium was replaced with fresh DMEM supplemented with 10% FBS.

Murine SMC Migration and Proliferation

The migration of murine aortic SMCs was assessed using the xCELLigence RTCA DP system as described above. Briefly, the electrode side of the membrane was coated with 0.1% gelatin. The bottom compartment of each well was filled with 165 µL of culture medium or serum-free medium as a control, and the membrane compartment was mounted. The upper wells were filled with 50 µL of serum-free medium and equilibrated for 1 hour at 37 °C in an incubator. Cell concentrations were adjusted to 2.7×10^4 cells/mL per well. Data were recorded for 24 hours. To quantify the proliferation of murine aortic SMCs, cells were seeded in 12-well plates to yield a confluence of ≈30%. To make these results comparable to those of the proliferation assay for human SMCs transfected with siRNA, the cells were incubated for 1 day (with 100-ng/mL murine PDGF-BB or without), with the time point 0 hour defined as 24 hours after seeding. Murine WT SMCs with a Zc3ch1 knockdown were seeded at 3000 cells/well in a 96-well plate in 75-µL DMEM with 10% FCS; after 2 to 4 hours, another 75-µL medium was added, and 0-hour photographs were taken, then every 24 hours. At each given time point, the cells were washed once with 1-mL PBS and fixed with 0.5 mL of 4% (v/v) paraformaldehyde for 5 minutes. After removing the paraformaldehyde, the cells were permeabilized with 0.5-mL Triton-X-100 for 10 minutes, washed with 1-mL PBS, and stained with 0.5-mL 4′,6-diamidino-2-phenylindole solution for 10 minutes in the dark. After acquiring images of 10 nonoverlapping regions per well, both the cell number and average size of nuclei were determined using our in-house Python script CellCounter.py. The results were normalized to time point 0 for each condition and replicate. The results were validated using the bromodeoxyuridine assay as described above. The incubation of bromodeoxyuridine was shortened to 4 hours. Proliferation assays were performed in 5 and 4 replicates, respectively.

Immunofluorescence and Confocal Microscopy

SMCs were seeded on µ-slide chamber slides (ibidi) and cultured in SMC medium (see above) containing 100-ng/mL murine PDGF-BB until the desired confluence. Both genotypes (Zc3hc1 knockout versus WT) were treated equally. After fixation with cold methanol-acetone solution, PDGF-treated SMCs (see above) were permeabilized with 0.2% Triton-X (1% BSA in PBS), and unspecific sites were blocked with 3.5% BSA. SMCs were stained with anti-NIPA (OriGene, AP20366PU-N, 1:100), anti-Tubulin (Abcam, ab6160, 1:1000) or anti-CCNB1 (Thermo Fisher Scientific, PA5-85113, 1:200), 4′,6-diamidino-2-phenylindole, and Alexa Fluor 568/Alexa Fluor 488. Images were acquired using a confocal microscope (Leica, TCS-SP5), and 8 to 10 z-stacks (≈1-µm distance) were combined for maximum intensity projections.

Statistical Analysis

All data are presented as the mean±SD, with 2 groups compared by the unpaired Student *t* tests or the Mann-Whitney *U* tests ($n<8$ or not normally distributed data). Normal distribution was confirmed using the Shapiro-Wilk test (as implemented in SciPy). The Welch *t* test was used when the assumption of equal variances was violated, defined as an SD ratio outside the interval 0.67 to 1.5. Group differences for $n=3$ per condition were assessed using the Welch *t* test and confirmed using 1-sided exact permutation tests as descriptive statistics to evaluate group differences. A Kruskal-Wallis test ($n>3$ per group) or ANOVA ($n=3$ per group) was applied if 2 conditions (with and without PDGF-BB) were tested. In the case of intergroup comparisons (ie, with and without PDGF treatment), Tukey-honest significant difference tests were applied to avoid inflation of type I error. Statistical significance for genetic associations was determined using a linear mixed-model regression. All statistical analyses were performed using R or Python libraries, with $P<0.05$ considered statistically significant.

RESULTS

Associations of the *ZC3HC1* Variant rs11556924-T With Cardiovascular Disease–Related Phenotypes

A hypothesis-free phenome scan was performed using the MR-Base PheWAS online tool[33] and the genome-wide association study catalog[34] to determine the associations of rs11556924 variants with cardiovascular disease–related phenotypes. As expected, a genome-wide significant association was observed between this single-nucleotide polymorphism and cardiovascular-related traits, including hypertension and CAD (Figure 1A; Table S1), with the rs11556924-T allele associated with reduced risk of these diseases. A suggestive association ($P=1.4\times10^{-5}$) was also observed between this single-nucleotide polymorphism and mean carotid IMT in the MRC-IEU consortium data (Table S1).

The rs11556924-T Single-Nucleotide Polymorphism Is Associated With Lower ZC3HC1 Expression and Higher Migration in Human Aortic SMCs

To understand the role of the rs11556924 variant at the level of gene expression, an expression quantitative trait locus analysis was performed using aortic SMCs of 151 human donors. This assay showed that the T allele was associated ($P=0.012$) with lower *ZC3HC1* expression (Figure 1B). We observed 5% and 10% reduction of *ZC3HC1* expression in SMCs heterozygous and homozygous for the T risk allele, respectively, compared with the homozygous carriers of the C non-risk allele. To our knowledge, there are no expressed quantitative trait loci in monocytes/macrophages[35] or aortic endothelial cells,[36] suggesting that the regulatory impact of rs11556924 in the *ZC3HC1* locus is SMC-specific (Table S2). Therefore, we assessed the impact of this variant on SMC migration, a hallmark of vascular remodeling.[17] Cell migration

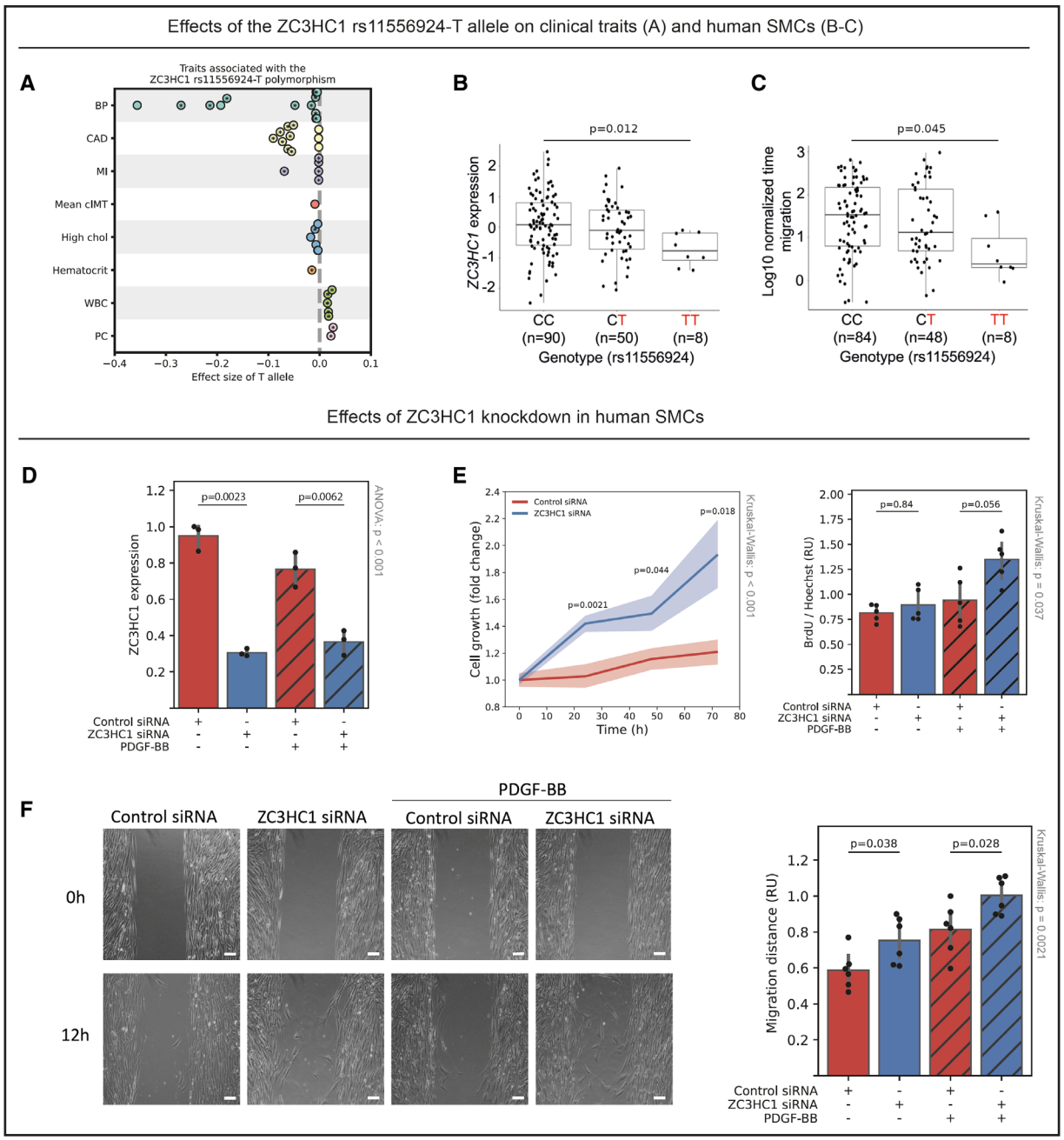

Figure 1. Association of rs11556924 with cardiovascular diseases predominantly driven by vascular smooth muscle cell (SMC) dysfunction, *ZC3HC1* expression, and vascular SMC phenotype.

A, Predominant association of rs11556924 with cardiovascular disease (CVD) driven by vascular SMC dysfunction. The plot shows the β values (effect size) of the rs11556924-T allele derived from several genome-wide association studies (GWASs) categorized according to 8 CVD-related traits. Asterisks indicate genome-wide significance ($P<5\times10^{-8}$); data points without asterisks represent genome-wide associations with suggestive significance ($P<5\times10^{-5}$). Negative effect sizes (reflecting β values derived from public GWAS summary statistics; Table S1) indicate that the risk allele (T) of the single-nucleotide polymorphism, rs11556924, is associated with a lower risk for several traits, including blood pressure (BP) or coronary artery disease (CAD). **B**, The risk allele (T) of rs11556924 is associated with lower *ZC3HC1* expression (transcripts per million [TPM]) and (**C**) faster migration by vascular SMCs. *P* values in **B** and **C** were determined using the linear mixed-model regression. SMCs transfected with siRNA against *ZC3HC1* showed significant (**D**) *ZC3HC1* downregulation, (**E**) higher PDGF (platelet-derived growth factor)–induced proliferation rate confirmed by counting nuclei stained with Hoechst 33342 dye (**left**, n=3, 6 images per replicate), as well as BrdU (bromodeoxyuridine) assay (**right**, n=5, mean of 3 to 4 wells per condition), and (**F**) increased migration in the presence or absence of PDGF-BB (n=6, means of 4 images per replicate). Representative images of migratory SMCs transfected with *ZC3HC1* siRNA and control siRNA are shown after 12 hours (scale bars, 100 µm). Values are shown as means. The translucent error bands represent 1 SD. *P* values in **D** were determined using the Welch *t* tests and confirmed using 1-sided exact permutation tests. *P* values in **E** and **F** were calculated using the Kruskal-Wallis tests, and 2 groups were compared by the Mann-Whitney *U* tests. Chol indicates cholesterol; cIMT, carotid intima-media thickness; MI, myocardial infarction; PC, platelet count; and WBC, white blood cell count.

assays were performed using 100-ng/mL PDGF-BB as a chemoattractant in serum-free media, as described previously.[19] SMCs carrying the rs11556924-T variant were found to migrate faster toward PDGF-BB than SMCs carrying the C allele (Figure 1C). The heterozygous and homozygous SMCs for the T risk allele migrate 10% and 50% faster, respectively, compared with the homozygous carriers of the C non-risk allele.

Downregulation of *ZC3HC1* in Human SMCs Increases Proliferation and Migration

To further investigate how *ZC3HC1* modulation affects SMC proliferation and migration, cells were transfected with siRNA against *ZC3HC1* (*ZC3HC1* siRNA). We ensured an RNA-level knockdown efficiency of ≈70% (Figure 1D), which was sufficient to achieve a corresponding reduction in protein levels (Figure S1). A lower level of *ZC3HC1* messenger RNA significantly enhanced the proliferation of SMCs (Figure 1E). Of note, no significant correlation was observed in SMCs derived from 151 human donors[19] between the T allele and cell proliferation at 24 hours (Figure S2). In agreement with the migratory response of the 151 SMC types, siRNA-mediated knockdown of *ZC3HC1* promoted cell migration (Figure 1F). Moreover, adding PDGF-BB (mimicking vessel injury) was accompanied by lower expression of *ZC3HC1* and increased migration in control SMCs, as expected (Figure 1D through 1F). An increase in the migration rate was also observed in *ZC3HC1* knockdown compared with control SMCs in the presence of PDGF-BB.

Transcriptional Profiling of *ZC3HC1* Downregulation in Human SMCs

To determine the transcriptional profile of *ZC3HC1* downregulation, transcriptome analysis using RNA-seq was performed in aortic SMCs in the presence or absence of 5-ng/mL PDGF-BB. After quality control and quantification, the number of expressed genes (defined as genes with >6 read counts in at least 20% of the samples) ranged from 16 880 under control conditions to 17 242 after treatment with PDGF-BB (Table S3). Principal component analysis identified 2 distinct clusters of samples, corresponding to the cells cultured under the 2 conditions with endogenous *ZC3HC1* expression and *ZC3HC1* downregulation (Figure S3). Furthermore, 3045 genes were differentially expressed (P_{adj}<0.05). Of these, 284 genes showed a $\log_2$(fold change) above 0.5 (median, 0.68), and 179 genes were downregulated with $\log_2$(fold change)<−0.5 (median, −0.67). The latter also includes the canonical SMC markers, *LMOD1*, *TPM1*, *CNN1*, *CALD1*, *ACTA2*, and *TAGLN* (Figure 2A and 2B). Downregulation of the expression of genes encoding SMC markers in response to *ZC3HC1* knockdown was confirmed by quantitative polymerase chain reaction (Figure 2C).

Network Analysis of Differentially Expressed Genes

Subsequent network analysis of differentially expressed genes (P_{adj}<0.05 and abs[$\log_2$(fold change)]>0.4) using the STRING database[27] revealed that the *CCNB1* gene encoding CCNB1 is a central hub for a variety of gene clusters (Figure 3A and 3B; Figure S4; Tables S4 through S6), whereas *ZC3HC1* interacts only with *CCNB1* (STRING score=0.607). Therefore, network analysis indicated that modulation of *ZC3HC1* predominantly induces transcriptional changes through CCNB1. Additional enrichment analysis of gene clusters highlighted several biological processes that were apparently modulated by the knockdown of *ZC3HC1*, including protein ubiquitination, muscle contraction/cytoskeleton organization, and cell division (Figure 3B). To test whether *CCNB1* is modulated by lower levels of *ZC3HC1* in SMCs, we performed coexpression and Western blot analyses. Analysis of gene expression in aortic SMCs of 151 individuals showed a positive correlation (R=0.59; P=1.4×10^{-15}) between *ZC3HC1* and *CCNB1* at the RNA level (Figure 3C, top). Similarly, quantitative polymerase chain reaction showed that siRNA-mediated *ZC3HC1* downregulation reduced *CCNB1* expression in SMCs (Figure 3C, top right). At the protein level, however, a lack of hNIPA resulted in the intracellular accumulation of CCNB1 (Figure 3C, bottom), as previously described.[10] To explain changes in the expression of SMC contractile marker genes (Figures 2C, 3A, and 3B), we analyzed protein levels of the transcription factor SRF, which is critical for maintaining the contractile phenotype of SMCs.[37] Indeed, the level of native SRF is significantly impaired in the presence of PDGF-BB in *ZC3HC1*-deficient SMCs (Figure 3D), indicating a *ZC3HC1-CCNB1-SRF* axis regulating the expression of SMC contractile marker genes (eg, *CNN1*). On the protein level, however, no significant changes could be observed for *CNN1* or *LMOD1* (Figure 3E), demonstrating the minor effects of short-term *ZC3HC1* silencing in SMCs.

Proteomic Analysis of SMC Proteins

In addition to RNAseq, we subjected cell lysates from SMCs carrying the T allele (n=7) or C allele (n=6) to proteomic analyses. Comparison of SMCs carrying the rs11556924-T allele (ZC3-T) versus SMCs carrying the rs11556924-T allele (ZC3-C) revealed that only 12 proteins show significantly lower protein levels in ZC3-T SMCs (Figure S5; Table S7). These proteins (eg, PDGF receptor beta) are seemingly involved in PDGF signaling (Enrichr[38]: BioPlanet 2019; P=0.003; q-value=0.08; odds ratio, 363.3) and cell chemotaxis (Enrichr: Gene

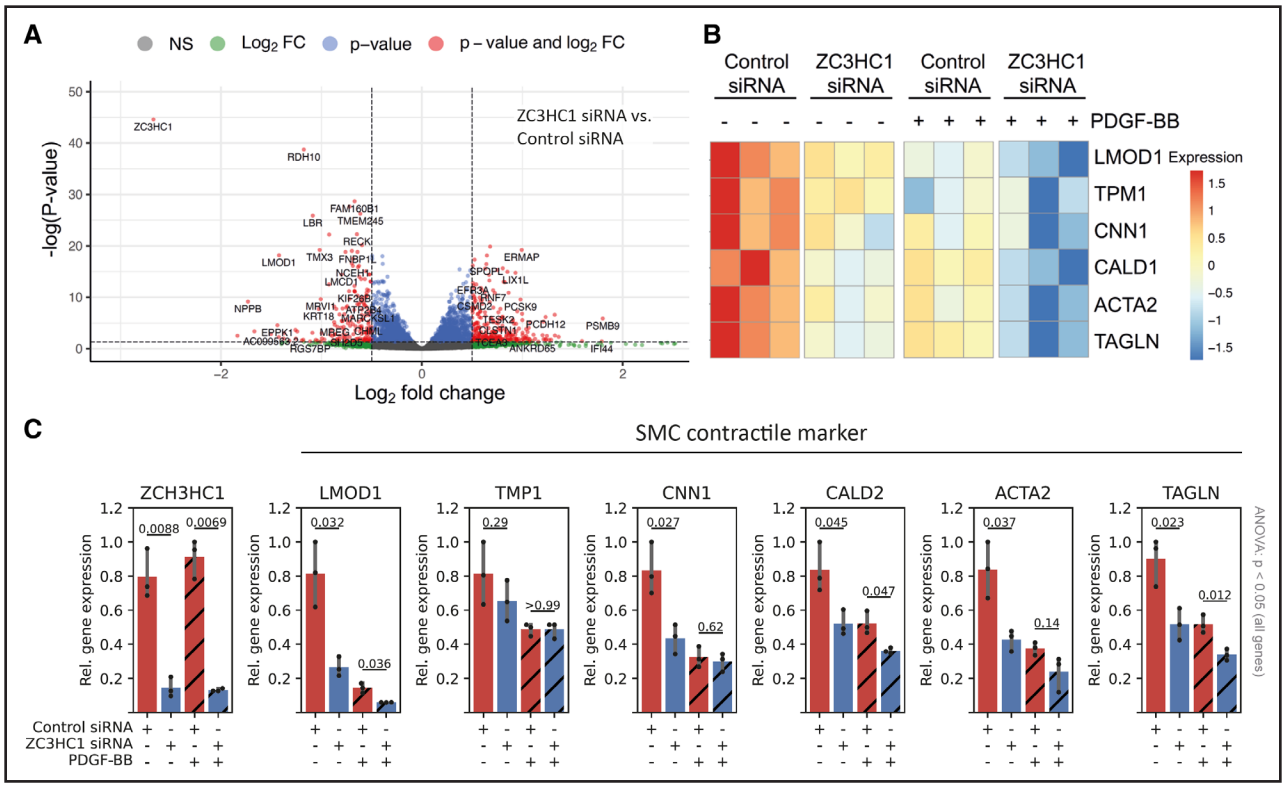

Figure 2. Transcription profiling of human smooth muscle cells (SMCs) after *ZC3HC1* (zinc finger C3HC-type containing 1) downregulation.

A, Volcano plot of the expression profiles of differentially expressed genes in SMCs transfected with siRNA against *ZC3HC1* (*ZC3HC1* siRNA; n=4) and control siRNA (n=6) using PDGF (platelet-derived growth factor)-BB treatment as covariate. The red data points represent the differentially expressed genes with statistical significance, whereas the gray data points indicate genes without disturbed gene expression. The vertical dashed lines correspond to a 0.5-fold change in gene expression (up or down), and the horizontal dashed line represents the adjusted *P* value for each gene. **B**, Heatmap showing contractile SMC marker genes that were differentially expressed upon knockdown of *ZC3HC1* (from one experimental batch, ie, 3 replicates per condition) in the presence or absence of PDGF-BB. **C**, Quantitative polymerase chain reaction (qPCR) validation of the expression of the contractile SMC marker genes. Values are shown as mean±SD. *P* values in **C** were determined using the Welch *t* tests and confirmed using 1-sided exact permutation tests.

ontology biological process; *P*=0.0008; q-value=0.06; odds ratio, 59.5).

Phenotyping of *Zc3hc1*$^{-/-}$ Mice

Like human *ZC3HC1* (Table S8), the murine homolog is ubiquitously expressed in various tissues (Figure S6A and S6B). X-Gal staining confirmed that transgenic mice harbored the *LacZ* gene (Figure S6C) with similar results observed at the DNA level using agarose gel electrophoresis for *LoxP* sites (Figure 4A). Phenotypically, the birth rate was lower for *Zc3hc1*$^{-/-}$ than for WT and heterozygous animals. In general, Zc3hc1$^{-/-}$ mice display reduced birth rate (males, 8%; females, 11.5%) and are infertile. In addition, knockout of *Zc3hc1* had a significant impact on body weight (Figure 4B, left), with lifetime body weight being significantly lower for *Zc3hc1*$^{-/-}$ than for WT (23±2 versus 27±5 g; *P*<0.0001 at 44 weeks; Figure S6D). In addition, a few *Zc3hc1*$^{-/-}$ mice exhibited shorter snouts than their WT littermates (Figure 4B, right). Despite the effect of *Zc3hc1* knockout on body weight, life span was similar in *Zc3hc1*$^{-/-}$ and WT mice (Figure 4B, bottom).

ZC3HC1 Deficiency Leads to Increased Neointima Formation as a Response to Injury in Mice

Because of the effects of *ZC3HC1* on the in vitro migration and proliferation of human SMCs, the role of *Zc3hc1* on neointima formation was assessed in vivo using a vascular injury model. Neointima formation was induced in *Zc3hc1*$^{-/-}$ and WT mice by wire injury of the femoral artery, and the extent of neointima formation was assessed after 14 days. Neointima formation was ≈2-fold greater in knockout than in WT mice (*P*=0.005), accompanied by an increase in intima-to-media ratio (*P*=0.003; Figure 4C). No major significant differences were observed in the vessel circumference between Zc3hc1$^{-/-}$ and littermate controls after injury (73.9±12.2 versus 61.5±20.6 μm^2; *P*=0.155). Although *ACTA2* gene expression was significantly decreased in human *ZC3HC1* knockdown SMC, histochemical analysis of femoral arteries sections suggests no difference in the abundance of ACTA2-positive cells, neither in the media nor in the neointima

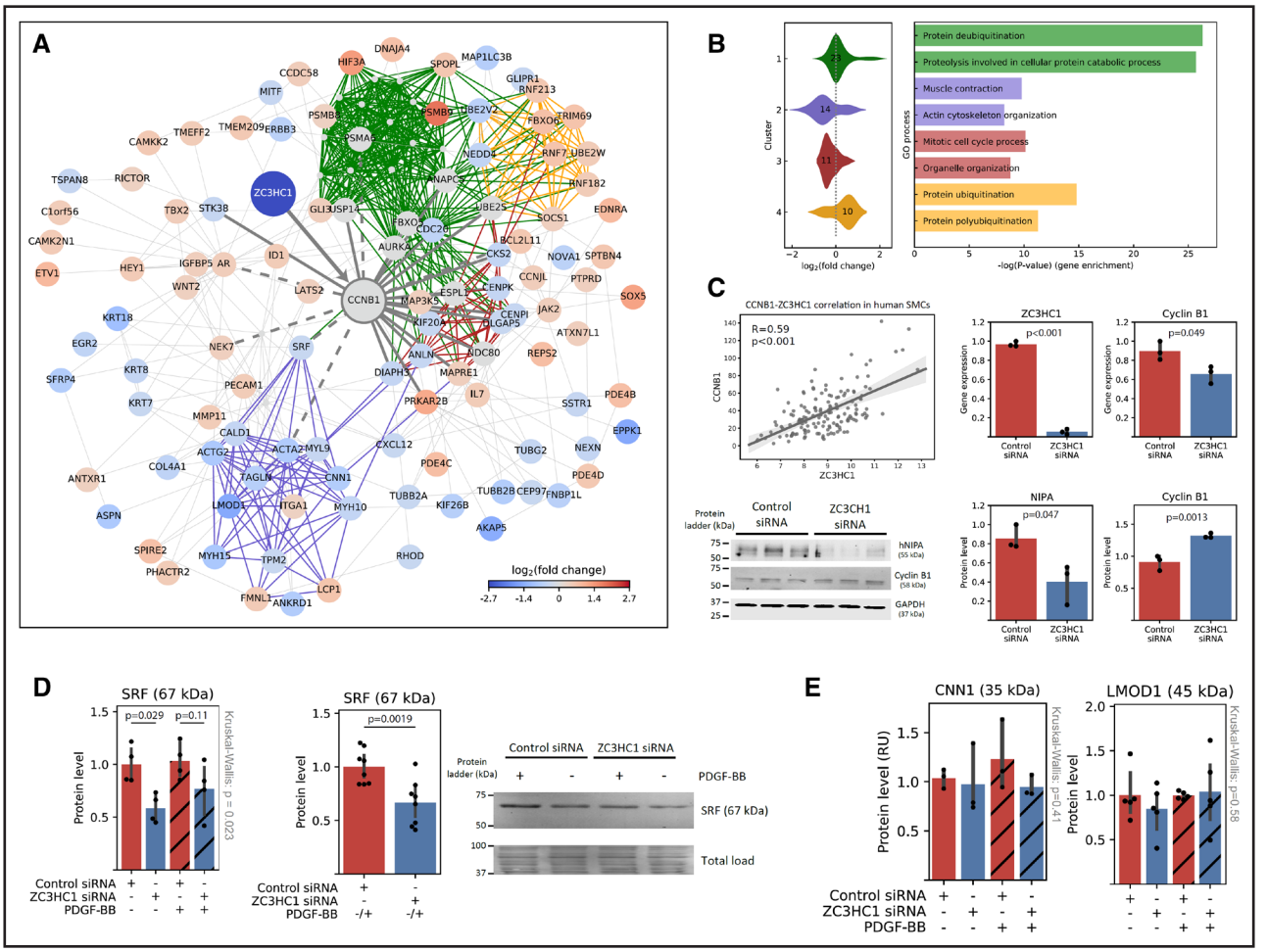

Figure 3. Gene interaction network of *ZC3HC1* (zinc finger C3HC-type containing 1)/CCNB1 (cyclin B1) in smooth muscle cells (SMCs) and accumulation of CCNB1 by *ZC3HC1* knockdown.

A, Effect of *ZC3HC1* knockdown on the CCNB1 subnetwork of differentially expressed genes (adjusted $P<0.05$ and abs[$\log_2$(fold change)] >0.4) derived from the STRING (Search Tool for the Retrieval of Interacting Genes/Proteins) database. The edges represent the combined STRING scores (>0.4; median=0.9) derived from coexpression, experimental, database, and text mining scores. The complete gene interaction network is shown in Figure S4. The fold changes in gene expression on the $\log_2$-scale are depicted by red and blue spheres. For example, SMC contractile marker genes (see purple cluster 2 in **A** and **B**) show lower gene expression (Figures 2B and 3B). Gray spheres indicate genes not differing in expression but interacting with CCNB1 or neighboring genes according to the STRING database. Gray bold lines indicate direct interactions with CCNB1 with medium to high confidence (scores >0.5), and dashed lines indicate direct interactions with lower confidence (score=0.4–0.5). Colored lines represent gene clusters. **B**, Distribution of $\log_2$(fold changes) in gene expression for each cluster and enriched biological processes derived from Gene Ontology (GO). Numbers in the violin plot indicate the number of genes in the cluster. **C**, Coexpression analysis in 151 human aortic SMCs' preparations showed a positive correlation between *ZC3HC1* and *CCNB1* gene expression, which was confirmed by transient knockdown of *ZC3HC1* and quantitative polymerase chain reaction (qPCR; right top corner). By contrast, the Western blot shows that *ZC3HC1* knockdown results in the accumulation of CCNB1 protein in SMCs. **D**, Western blot analysis of SRF (serum response factor) confirmed a significant reduction of SRF protein level in ZC3HC1-deficient SMCs in the presence of PDGF (platelet-derived growth factor)-BB. **E**, For CNN1 (calponin 1) and LMOD1 (leiomodin 1), only a small trend toward lower protein levels has been observed in ZC3HC1 knockout SMCs. Values of bar plots are shown as mean±SD. *P* values of bar plots in **C** were determined using the Welch *t* tests. *P* values in **D** and **E** were calculated using the Kruskal-Wallis tests, and 2 groups were compared by the Mann-Whitney *U* tests.

between knockout and WT mice (Figure 4D). The SMC-specific marker LMOD1 points toward a significantly higher SMC content in the neointima in *Zc3hc1* knockout mice versus WT mice (Figure 4E). In line, we found fewer CD31-positive cells (endothelial cells) in the neointima in the knockout than in the WT mice and slightly more Ki-67 positive cells in the G2 and M phase (Figure 4E) although the results were not statistically significant. These results indicate that vascular remodeling after injury is predominantly driven by the migration of medial SMCs.

Murine *Zc3hc1* Knockout SMCs Are Contractile, Less Proliferative, and More Migratory

Based on the findings from human SMCs, we isolated primary aortic SMCs from mice (female and male; Figure S7) and tested whether NIPA deficiency in murine

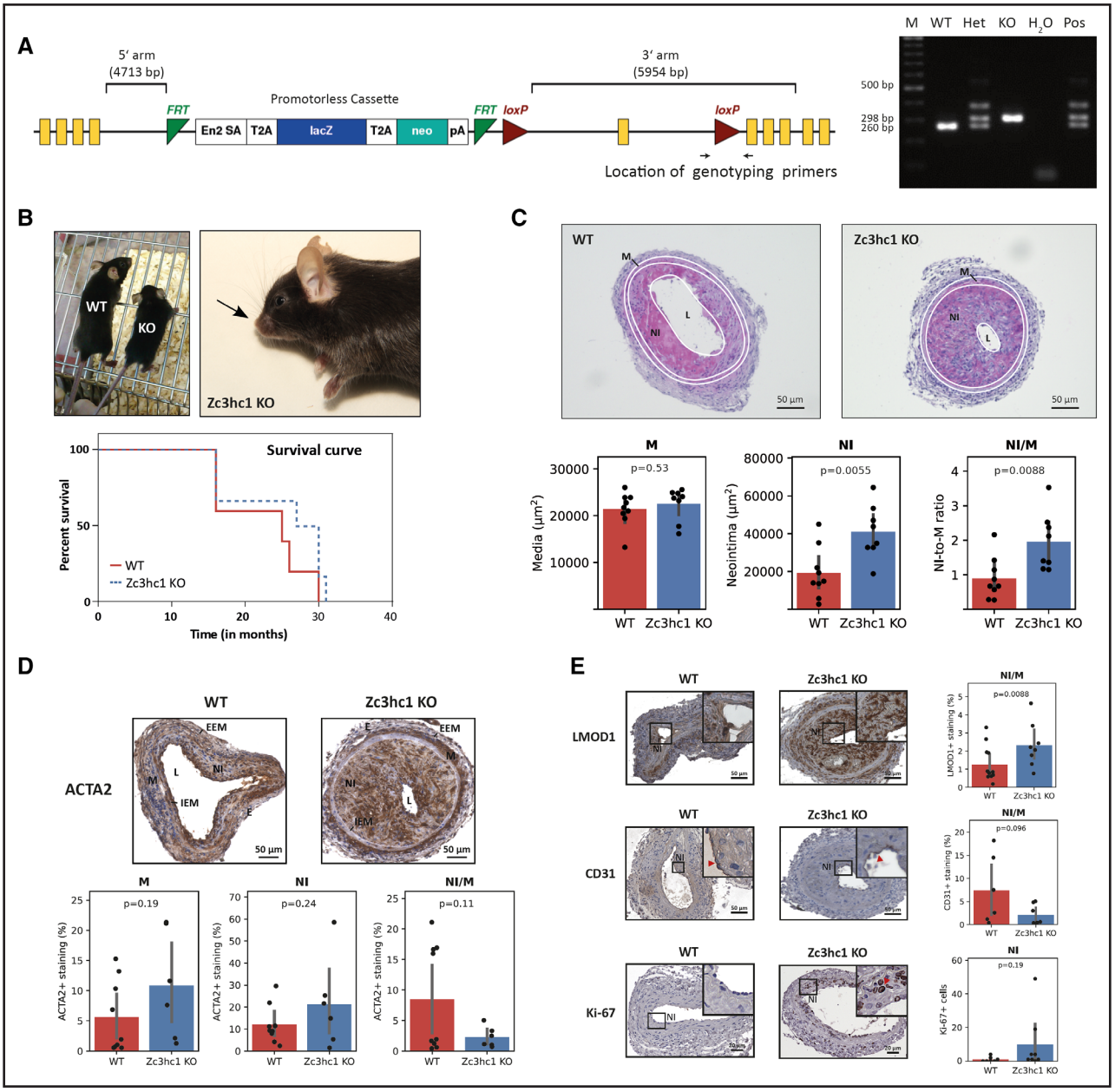

Figure 4. Generation and characteristics of *Zc3hc1* (zinc finger C3HC-type containing 1)−/− knockout (KO) mice.
A, Targeting vector used to generate *Zc3hc1*$^{-/-}$ mice (**left**) and genotyping of mice by polymerase chain reaction (PCR; **right**; M: 100-bp marker, wild-type [WT] mice [or *Zc3hc1*$^{+/+}$]; Het: heterozygous mice [*Zc3hc1*$^{\pm}$]; and Zc3hc1 KO mice [or *Zc3hc1*$^{-/-}$]; H_2O; and Pos: positive control represented by Het mice [*Zc3hc1*$^{\pm}$]). Location of genotyping primers. Primer pair targeting the intron between exons 5 and 6 of *Zc3hc1*, which contains a *loxP* site (**left**) in the targeted allele. The sizes of the PCR products were 298 bp in KO (*Zc3hc1*$^{-/-}$) and 260 bp in WT (*Zc3hc1*$^{+/+}$) mice, with Het mice (*Zc3hc1*$^{\pm}$) possessing both alleles. **B**, Decreased body weight (**left**) and abnormally short snout (indicated by arrow; **right**) in KO mice. The survival curve showing no statistically significant difference between KO (n=6) and WT (n=5) mice. **C**, Representative hematoxylin and eosin-stained femoral artery sections (**top**) and quantification of media area (M), area of neointima (NI), and neointima-to-media ratios (NI/M; **bottom**) in female WT (n=9) and female KO (n=8) mice. Scale bars, 50 µm. **D**, ACTA2 (smooth muscle actin alpha 2)-positive cells predominantly reside in the media (M) and in the neointima (NI) in both WT and Zc3hc1 KO mice (E, externa; EEM, external elastic membrane; and IEM, internal elastic membrane). **E**, Tissue slides were stained with anti-LMOD1 (leiomodin 1; smooth muscle cell [SMC] marker), anti-CD31 (endothelial cell marker), or anti-Ki-67 (proliferation marker) antibody. Primary antibodies were visualized using a horseradish peroxidase system and DAB (3,3′-diaminobenzidine) staining solution. A detailed description can be found in the main text. Values of the bar plots are shown as mean±SD. *P* values in **C** and **E** (LMOD1) were calculated using unpaired Student *t* tests. *P* values in **D** and **E** (CD31 and Ki-67) were determined using the Mann-Whitney *U* tests.

primary aortic SMCs modifies migration and proliferation. Compared with WT SMCs, the migration of *Zc3hc1*$^{-/-}$ SMCs was significantly enhanced at 12 hours (*P*=0.04) but not at later time points (Figure 5A). Furthermore, the proliferation of *Zc3hc1*$^{-/-}$ SMCs was significantly diminished than that of WT SMCs (Figure 5B). This effect is

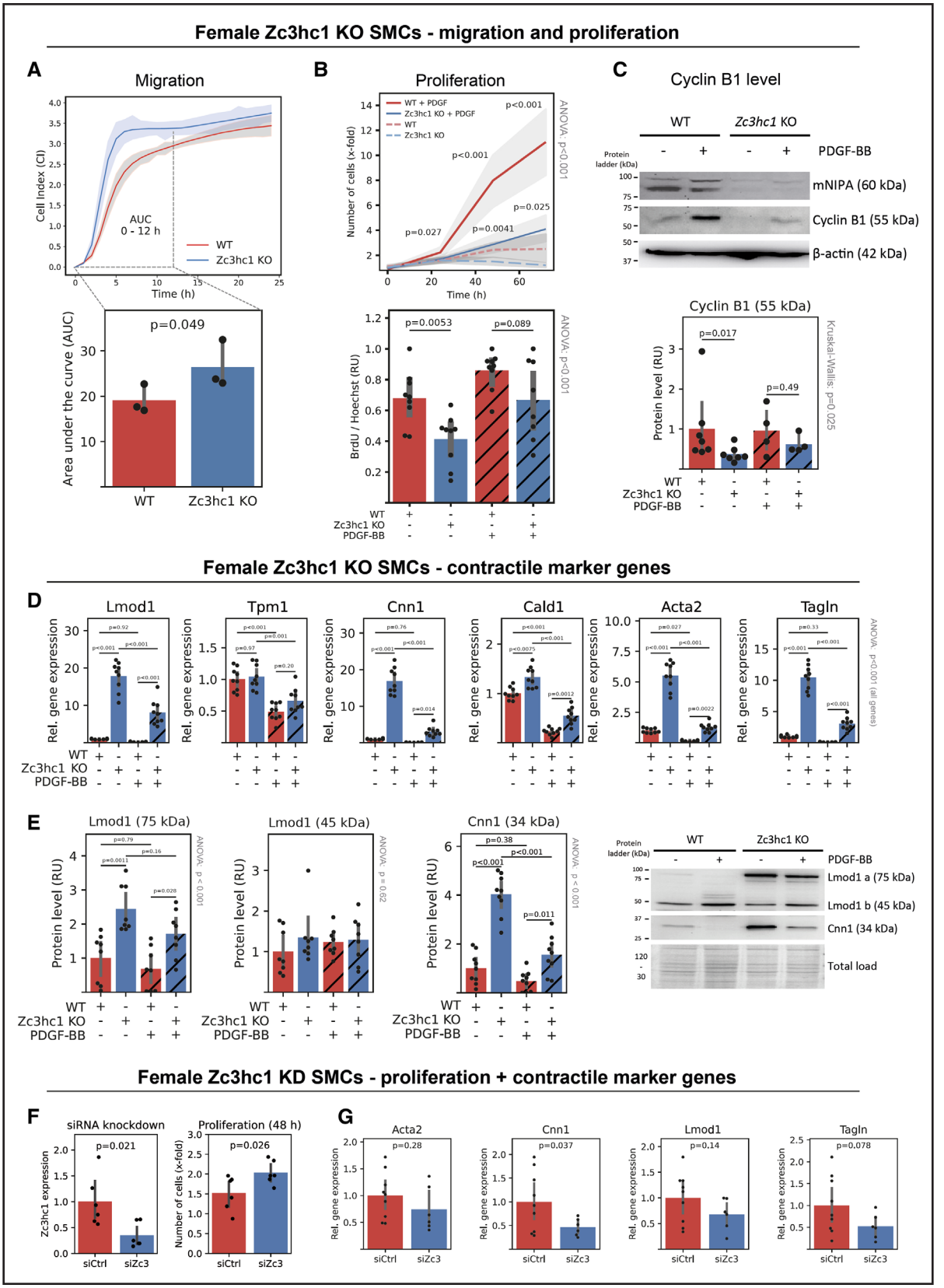

Figure 5. Knockout (KO) and knockdown (KD) of *Zc3hc1* (zinc finger C3HC-type containing 1) in murine aortic smooth muscle cells (SMCs).

SMCs isolated from female *Zc3hc1* KO mice show elevated migration in the first 12 hours (**A**) but less proliferation (**B**) compared with SMCs isolated from wild-type (WT) mice. **C**, Western blotting of mNIPA (mouse NIPA protein; encoded by *Zc3hc1*) confirms the knockout of *Zc3hc1* in SMCs, resulting in reduction of cyclin B1 protein. **D**, Relative messenger RNA (mRNA) levels are shown for contractile (*Continued*)

enhanced in PDGF-BB–induced proliferation. Because NIPA has been shown to interact with CCNB1,[10] we compared the expression of CCNB1 protein in NIPA-deficient and WT murine SMCs. In line with decreased proliferation, *Zc3hc1*$^{-/-}$ SMCs show significantly reduced CCNB1 levels compared with WT SMCs (P=0.043; Figure 5C). Furthermore, *Zc3hc1*$^{-/-}$ SMCs exhibit a contractile signature reflected by enhanced gene expression of almost all SMC contractile marker genes (Figure 5D) and higher protein levels of *Lmod1* and *Cnn1* (Figure 5E). This contractile SMC phenotype was observed in female SMCs (Figure 5) and, to a lesser extent, in male SMCs lacking *Zc3hc1* (Figure S7). A transient knockdown of Zc3hc1, however, resulted in increased proliferation, accompanied by reduced activity of contractile marker genes as observed in the human counterpart (Figure 5F and 5G).

CCNB1 and mNIPA Are Located at Similar Sites During Mitosis

To further understand the mechanistic link between *ZC3HC1*/NIPA, CCNB1, and cell migration/proliferation, we captured the location of both proteins during the cell cycle in murine SMCs using confocal microscopy. During interphase, mNIPA is predominantly located in the nucleus but also appears to be present in the cytoplasm where it colocalizes to some degree with microtubules (Figure 6). During mitosis, mNIPA seems to be located either in fragmented nuclear membranes[39,45] in prophase or at the cleavage furrow during anaphase and telophase. On the contrary, CCNB1 is mainly present outside the nucleus in small amounts (Figure 7). The level of CCNB1 starts to rise during the G2 phase, and CCNB1 accumulates in the nucleus during the G2 to M phase transition.[46] In the prometaphase and metaphase, CCNB1 appears to overlap with components of the spindle apparatus (eg, centrosomes[42] and microtubules[43]). Similar to mNIPA, CCNB1 appears to be located directly at the contractile actomyosin ring[44] during telophase and cytokinesis. Of note, a similar colocalization of hNIPA and CCNB1 during late mitosis and cytokinesis was also observed in primary human SMCs (Figure S9). No obvious structural differences were observed between mitotic WT SMCs and *Zc3hc1* knockout SMCs for CCNB1. However, there is a tendency toward more plasma membrane blebbing in *Zc3hc1* knockout SMCs during (pro)metaphase (Figure 7B). To estimate the proportion of SMCs in different cell-cycle states, we counted SMCs in G2 phase, G2-M transition, and M phase (Figure 7C). A total of 144 images were analyzed using an in-house Python script that uses staining intensity and location (nucleus versus cytoplasm) of CCNB1 to assign the different phases. In accordance with lower proliferation rates of murine *Zc3hc1*$^{-/-}$ SMCs, the number of nuclei is lower in *Zc3hc1*$^{-/-}$ SMCs than in WT SMC (673±131 versus 1143±131), as is the percentage of SMCs undergoing G2 (4.3±1.2% versus 18.4±3.8%), G2-M transition (0.8±0.4% versus 3.3±1.0%), or mitosis (0.6±0.4% versus 1.9±0.6%). Interestingly, the proportion of SMCs undergoing mitosis versus SMCs in G2/G2-M transition phase is higher in *Zc3hc1*$^{-/-}$ SMCs than in WT SMCs, providing weak evidence that the absence of *Zc3hc1*/mNIPA results in a longer mitosis phase.

DISCUSSION

Neointima formation, a hallmark of restenosis, is one of the main clinical complications in patients who undergo coronary artery revascularization.[47,48] Vascular SMCs, essential for vessel tone and structural integrity, play a pivotal role in this process by switching from a contractile to a migratory and proliferative phenotype in response to injury or inflammation.[49–51] In this study, we identify the cell cycle–related CAD-gene *ZC3HC1*, which encodes NIPA, as a key regulator of this process.

The CAD-protective rs11556924-T allele[2–8] reduces *ZC3HC1* gene expression as shown in GTEx and aortic SMCs from 151 heart transplant donors[19] and is associated with impaired NIPA activity.[7] SMCs carrying this allele exhibit increased migratory capacity, a finding not seen in other vascular cell types, including monocytes/macrophages,[35] endothelial cells,[36] or blood samples,[11] highlighting SMC-specific effects, as previously reported by our group.[52] The siRNA-mediated knockdown of ZC3HC1 in human SMCs replicated this phenotype, increasing both migration and proliferation, accompanied by CCNB1 accumulation, impaired expression of contractile marker genes (eg, *ACTA2*, *CNN1*, *TAGLN*, and *LMOD1*), and enhanced expression of genes involved in ECM (extracellular matrix) organization and cytokine signaling. Furthermore, transcriptomic and pathway analysis revealed that *ZC3HC1* deficiency promotes a proliferative SMC phenotype, potentially via SRF suppression and altered protein ubiquitination. While global transcriptomic changes were modest, the shift in phenotype suggests that posttranscriptional regulation and protein-level effects, including nuclear pore dynamics and mitotic spindle function, may be crucial.

Figure 5 Continued. SMC marker genes. Values were normalized to WT without PDGF (platelet-derived growth factor)-BB (mean=1). **E**, Western blot analyses of LMOD1 (leiomodin 1) and CNN1 (calponin 1) with a representative Western blot shown right (total load=amido black staining). **F**, Transient KD of Zc3hc1 (siZc3 [small interfering RNA targeting Zc3hc1]) results in more proliferation after 48 hours compared with scrambled siRNA (siCtrl) and (**G**) reduced expression of contractile marker genes. The translucent error bands (**A** and **B**) represent 1 SD. Values of bar plots are shown as mean±SD. *P* values in **A**, **B**, and **G** were calculated using the unpaired Student *t* tests. *P* values in **D** and **E** were calculated using Tukey-honest significant difference (HSD) tests. *P* values in **C** and **F** were determined using the Mann-Whitney *U* tests.

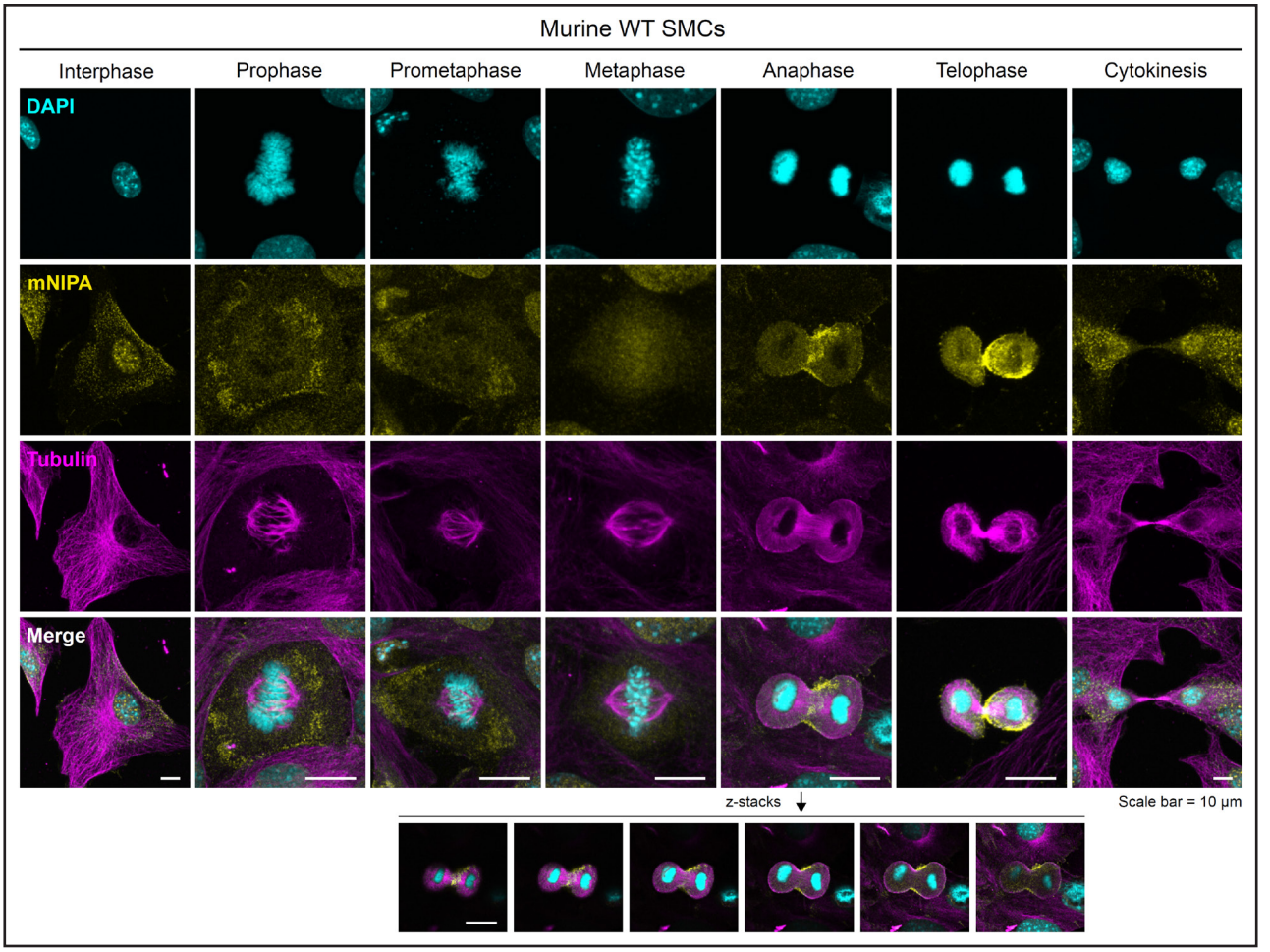

Figure 6. Localization of mNIPA (mouse NIPA protein) in murine aortic smooth muscle cells (SMCs) during the cell cycle. Pseudocolored confocal immunofluorescence images are maximum intensity projections of z-stacks (≈1-µm distance). PDGF (platelet-derived growth factor)-BB–treated murine wild-type (WT) SMCs were stained with 4′,6-diamidino-2-phenylindole (DAPI; cyan), anti-NIPA (nuclear interaction partner of anaplastic lymphoma kinase; yellow), and anti-tubulin (magenta). During interphase, mNIPA is predominantly located in the nucleus but is also colocalized to some extent with microtubules. During the initial stage of mitosis (prophase/prometaphase), mNIPA appears to be located at fragmented nuclear membranes.[39] Later during the metaphase, anaphase, and early telophase, mNIPA is predominantly situated in the cleavage furrow and contractile ring. The location of mNIPA during the anaphase is highlighted in **bottom**.

To validate our findings in vivo, Zc3hc1$^{-/-}$ mice showed exaggerated neointima formation after vascular injury, accompanied by enhanced SMC migration and reduced endothelial coverage. However, as a complete knockout model was used, we cannot rule out contributions from endothelial cells. Indeed, CD31 staining was decreased (Figure 1E), suggesting that endothelial regeneration may also be impaired. Interestingly, SMCs isolated from Zc3hc1$^{-/-}$ mice displayed decreased proliferation and CCNB1 levels, contrasting with the effects observed after partial knockdown, indicating a dose-dependent or biphasic effect of *Zc3hc1*. Consistently, transient *Zc3hc1* knockdown in WT murine SMCs recapitulated the proliferative phenotype observed in human SMCs, further validating this model.

To find plausible explanations for this discrepancy, we mapped the location of NIPA during mitosis using confocal microscopy, revealing indirect colocalization of mNIPA and CCNB1 during mitosis, especially at the nuclear envelope and cleavage furrow (Figures 6 and 7; Figure S9). These findings indicate that mNIPA (and its human ortholog) not only regulates mitotic entry but is also crucial for proper mitotic exit by regulating cellular fission. While partial deficiency of mNIPA accelerates CCNB1 accumulation in G2 phase and mitotic entry, the complete loss of mNIPA may disrupt mitotic processes either due to a lower level of CCNB1 or dysregulation of its degradation (Figure 5C). For instance, degradation of CCNB1 by the APC/C (anaphase-promoting complex/cyclosome) is required for cleavage furrow formation. The localization of mNIPA at the cleavage furrow indicates that mNIPA might also be crucial in this process. Besides APC/C, mNIPA might also be involved in the degradation of CCNB1 before cleavage furrow formation. Therefore, it is plausible that the lack of mNIPA can be responsible for impaired cytokinesis

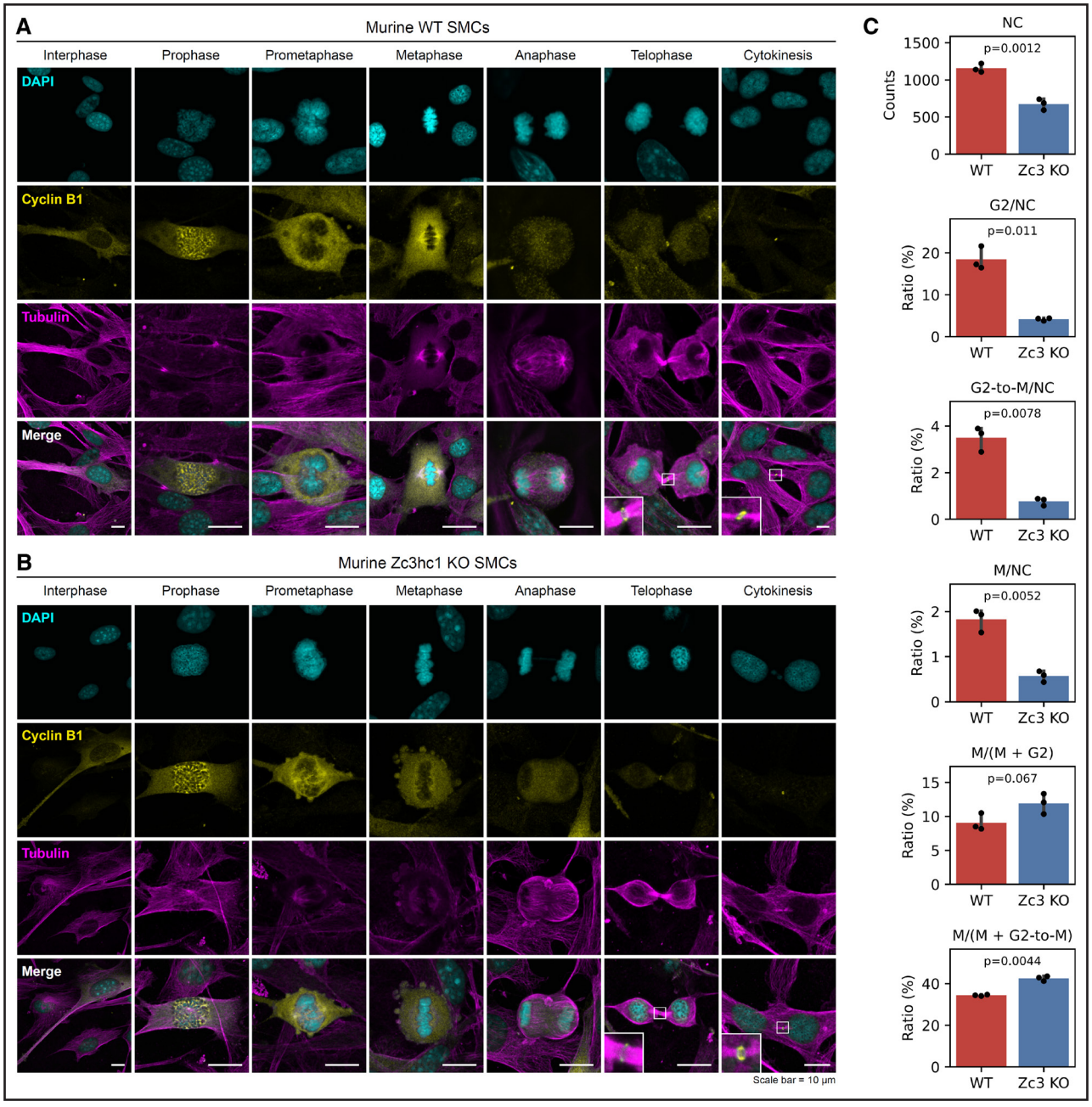

Figure 7. Localization of cyclin B1 in murine aortic smooth muscle cells (SMCs) during the cell cycle.
Pseudocolored maximum intensity projections of confocal immunofluorescence z-stacks (≈1-µm distance) show PDGF (platelet-derived growth factor)-BB treated (**A**) wild-type (WT) and (**B**) *Zc3hc1* (Zc3) knockout (KO) murine SMCs stained with 4′,6-diamidino-2-phenylindole (DAPI; cyan), anti-cyclin B1 (yellow), anti-tubulin (magenta), and respective secondary antibodies. During interphase, cyclin B1 resides in the cytoplasm at low levels. At early prophase, cyclin B1 is accumulated in the nucleus where it is involved in the disassembly of nuclear pore complexes[40] and depolymerization of nuclear lamin filaments through phosphorylation.[41] During prometaphase and metaphase, cyclin B1 overlaps partly with components of the spindle apparatus (centrosomes[42] or spindle assembly checkpoints[43]). In the late stage of mitosis (telophase) and during cytokinesis, cyclin B1 appears to be directly located at the contractile actomyosin ring[44] (enlarged sections). **C**, The number of nuclei (NC) of murine SMCs (WT vs Zc3 KO) and the number of murine SMCs in G2 phase (based on cyclin B1 level), in the G2 to M phase transition (G2-to-M), and SMCs in mitosis (M). A total of 144 images per genotype from 3 replicates taken with a 10× objective were analyzed semiautomatically using an in-house Python script (available upon request). A detailed description of this analysis can be found in Figure S10. Values of bar plots are shown as mean±SD. *P* values were determined using the Welch *t* tests.

and mitotic delay, also explaining increased membrane blebbing found in *Zc3hc1*$^{-/-}$ SMCs (Figure 7B). Despite this reasonable explanation, it remains still elusive why a knockout of *Zc3hc1* abrogated proliferation in murine SMC under PDGF-BB treatment but results in increased injury-induced neointima formation in vivo. The neointima buildup in Zc3hc1$^{-/-}$ mice might be caused by migratory SMCs (Figure 5A) that tend to be hypertrophic (enlarged

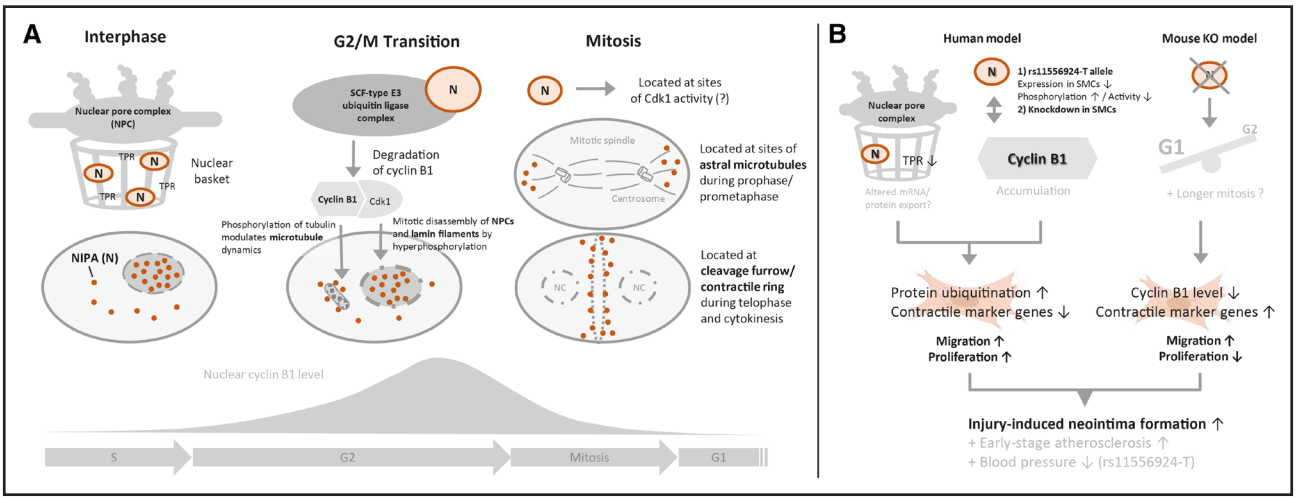

Figure 8. Diagram illustrating the proposed mechanisms of ZC3HC1 (zinc finger C3HC-type containing 1)/NIPA (nuclear interaction partner of anaplastic lymphoma kinase) modulation based on the main findings of this study and literature review. **A**, NIPA (N) is part of the nuclear pore complex[15] and the SCF (Skp, Cullin, F-box containing complex)–type E3 ubiquitin ligase complex.[7,10] During mitosis, NIPA appears to be located at sites of cyclin B1/Cdk1 (cyclin-dependent kinase 1) activity,[46] including nuclear pore complexes,[40] astral microtubules,[64,65] and cleavage furrow.[44,66] **B**, Under normal (healthy) conditions, NIPA activates the degradation of cyclin B1 during G1, S, and early G2 phases. However, *ZC3HC1* modulation by reducing the amount of NIPA or increasing NIPA phosphorylation[7,11] is accompanied by cyclin B1 accumulation and increased smooth muscle cell (SMC) migration and proliferation, which might also be mediated by dysfunctional nucleocytoplasmic transport of messenger RNAs (mRNAs) and proteins through less recruitment of TPR (translocated promoter region, nuclear basket protein) coiled–coil polypeptides.[15] This, in turn, leads to injury-induced neointima formation and progression of early stage atherosclerosis.[49,55–57] The rs11556924-T is associated with lower blood pressure (Figure 1A), and increased SMC proliferation in the late stage of atherosclerosis may contribute to plaque stability,[57,59] resulting in an asymptomatic progression of this disease. However, the complete lack of Zc3hc1 in murine SMCs results in reduced levels of cyclin B1 and cell-cycle arrest, presumably in the M/G1 phase. Therefore, neointima formation in Zc3hc1 knockout (KO) mice is most likely a consequence of SMC migration rather than cell proliferation. Illustrations of cells are from BioRender.com.

cell size) due to increased synthesis and accumulation of contractile proteins (Figure 5D and 5E). *Zc3hc1*$^{-/-}$ SMCs may also exhibit increased proliferation in vivo within the neointima, potentially driven by growth factors other than PDGF. Consistently, vessel sections from *Zc3hc1*$^{-/-}$ mice showed a trend toward a higher proportion of Ki-67–positive cells. The primary structural difference between murine and human arteries is that murine vessels typically lack intimal SMC. Consequently, the suitability of the mouse as a model for studying injury-induced neointima formation in humans remains debatable because proliferation of intimal SMCs is a central driver of neointimal thickening. However, it is also well described that in humans, medial injury of the internal elastic lamina results in migration of medial SMCs, and the medial fracture length of the internal elastic lamina strongly correlates with later neointimal thickness after stenting.[53,54] Finally, it remains unclear why the T allele in *ZC3HC1* lowers the risk of clinically symptomatic CAD[4,6,11,12] yet increases the risk of carotid IMT, as recently demonstrated in 502 patients with rheumatoid arthritis.[13] One reason could be the bivalent role of vascular SMCs as their biological function in atherosclerosis has opposite effects depending on the stage of the lesions (early versus advanced stage). At early stages of the formation of atherosclerotic lesions and during in-stent restenosis, migratory and proliferative SMCs are known to play a detrimental role in the progression of atherosclerosis.[49,55–57] Therefore, antiproliferative therapies were previously proposed.[58,59] On the contrary, the role of SMCs in advanced lesions is thought to be beneficial by stabilizing the plaque, which may result in an asymptomatic progression of atherosclerosis. Interestingly, 2 working groups observed that SMCs derived from advanced plaques are less proliferative. Consequently, they assumed that enhancement and not inhibition of SMC proliferation might be beneficial for plaque stability in advanced lesions,[57,59] thereby reducing the risk of major adverse cardiovascular event outcomes such as myocardial infarction. Taken together, the T allele leads to both lower levels and impaired activity of *ZC3HC1*/NIPA, resulting in migratory/proliferative SMCs that may worsen atherosclerosis at early stages, due to intimal thickening and lesion growth, but supports stability in advanced lesions through fibrous cap formation. In addition, the T allele's link to lower blood pressure may further reduce CAD risk[60,61] by enhancing SMC contractile responsiveness. To assess further human relevance, we analyzed publicly available single-cell and bulk RNAseq data sets from Gene Expression Omnibus (GSE159677, GSE28829, GSE120521, and GSE163154) and from the integrated single-cell atlas of human atherosclerotic plaques[62] (Figures S11 through S13). *ZC3HC1* expression is low in atherosclerotic cells but is predominantly

detected in nonproliferating SMCs that produce ECM, as well as in endothelial cells and T cells, supporting that *ZC3HC1* is required to control the cell cycle and prevent enhanced proliferation in lesional SMCs. Moreover, these data indicate that reduced *ZC3HC1* may drive early lesion development (Figure S11B). However, we found no convincing evidence that reduced levels of *ZC3HC1* directly contribute to plaque stability. In addition, we reanalyzed single-cell RNAseq data (GSE210248) obtained from pulmonary artery tissue of patients with pulmonary arterial hypertension and from control lung donors to characterize *ZC3HC1* expression patterns during pulmonary artery remodeling (Figure S13).[63] In line with single-cell data from atherosclerotic plaques, *ZC3HC1* levels are higher in nonproliferating, collagen-producing SMCs of pulmonary arterial hypertension tissue compared with control arterial tissue, suggesting that *ZC3HC1* may promote ECM production in SMCs and, thereby, contribute to vessel stiffness. Therefore, it is more plausible that the *ZC3HC1* T allele lowers CAD risk by reducing *ZC3HC1* expression and NIPA activity, thereby altering SMC contractility and ECM remodeling, and ultimately lowering blood pressure (a major CAD risk factor), rather than by stabilizing atherosclerotic lesions through enhanced SMC migration or proliferation. Because *ZC3HC1* is also expressed in endothelial cells, T cells, and mast cells, other inflammatory processes might also explain the association of *ZC3HC1* variants and CAD, neointima formation, or blood pressure. In conclusion, our integrative analyses highlight *ZC3HC1* as a neointima formation–associated gene with potential relevance for SMC-targeted therapeutic strategies. However, the role of NIPA in cell-cycle regulation and SMC biology seems to be more complex than previously anticipated. Its function spans multiple cell-cycle compartments, including the SCF complex, nuclear pore complex, and cleavage furrow; different phosphorylation sites, the tight regulation between NIPA and CCNB1 (NIPA phosphorylation by CCNB1-cyclin–dependent kinase 1 versus CCNB1 ubiquitination by NIPA), and their coexpression pattern (ZC3HC1 and CCNB1) suggest multilayered control of SMC phenotype. Figure 8 summarizes our proposed model of *ZC3HC1*/NIPA modulation, integrating current findings with established literature.

In summary, ZC3HC1/NIPA plays a complex, context-dependent role in SMC phenotype modulation, with implications for both atherosclerosis and restenosis. Our findings support *ZC3HC1* as a candidate regulator of vascular remodeling and underscore the need for refined models, such as lineage-tracing or humanized knock-in mice, to dissect its functions in specific vascular cell types.

Limitations

The number of studies showing an association between *ZC3HC1* and intima-media thickening in inflammatory conditions such as rheumatoid arthritis is limited. Also, the number of patients (n=500) included is low. Therefore, more human cohorts with more cases of IMT are desirable. Furthermore, we cannot rule out any sex bias for the development of IMT because only female mice were included in our study. However, we did not see any sex-stratified effects in our human data set or data sets from the UK Biobank (Table S9). Considering the proposed multiple functions of *ZC3HC1*/NIPA, a complete knockout model should be extended toward an SMC/EC-lineage-tracing mouse model in which *Zc3hc1* is only transiently or moderately modulated in a cell-specific manner. Moreover, a knock-in mouse will be the ideal model to study the exact role of the rs11556924-T/C.

ARTICLE INFORMATION

Received September 08, 2025; accepted February 11, 2026.

Affiliations

Institute for Cardiogenetics, Universität zu Lübeck, Germany (R.A., T.R., M.O., J.A.-H., M.L.M.-V., Z.A.). DZHK Partner Site North (German Centre for Cardiovascular Research) (R.A., T.R., M.O., J.A.-H., M.L.M.-V., Z.A.). University Heart Centre Lübeck, Germany (R.A., T.R., M.O., J.A.-H., M.L.M.-V., Z.A.). Immunology Center of Georgia (R.A.) and Department of Pharmacology and Toxicology (R.A.), Medical College of Georgia, Augusta University. A.I. Virtanen Institute for Molecular Sciences, University of Eastern Finland, Kuopio (R.A.). Deutsches Herzzentrum München, Technische Universität München and DZHK (German Centre for Cardiovascular Research) (J.W., H.S., T.K.). Partner Site Munich Heart Alliance, Germany (J.W., H.S., T.K.). Department of Internal Medicine III–Cardiology and Angiology, Saarland University Medical Center, Homburg, Germany (T.K.). Homburg Institute for CardioRenalMetabolic Medicine, Saarland University, Germany (T.K.). King's British Heart Foundation Centre, King's College London, United Kingdom (X.Y.). National Heart and Lung Institute, Imperial College London, United Kingdom (M.M.). Department of Anesthesiology and Perioperative Medicine (M.C.), Institute for Precision Health (M.C.), and Department of Human Genetics (M.C.), David Geffen School of Medicine, University of California, Los Angeles. Molecular Biology Institute, University of California, Los Angeles (M.C.).

Acknowledgments

The authors dedicate this work to the memory of Prof Dr rer nat Jeanette Erdmann (July 2023). Her scientific vision and lasting impact on this study remain invaluable. Her commitment to advancing cardiovascular genetics was fundamental to the conception and development of this study. The authors thank Annett Liebers, Maren Behrensen, Sandra Wrobel, and Lisa Diner for their technical support. The authors thank Jan Wenzel (Institute of Pharmacology and Toxicology, University of Lübeck) for technical assistance with confocal microscopy. The authors also thank the members of the Schunkert and Civelek laboratories for their feedback and constructive discussions.

Author Contributions

R. Aherrahrou, T. Reinberger, H. Schunkert, T. Kessler, and Z. Aherrahrou designed the project. R. Aherrahrou, T. Reinberger, Jeanette Erdmann, and Z. Aherrahrou contributed to the text of the main manuscript. R. Aherrahrou, T. Reinberger, J. Al-Hasani, J. Werner, M. Otto, and Z. Aherrahrou performed the characterization experiments and generated data for most of the figures and tables. M.L. Munoz-Venegas, M. Civelek, and T. Kessler participated in data analysis and lookup. All authors contributed to the final article.

Sources of Funding

This work was supported by the German Federal Ministry of Education and Research (BMBF) in the context of the German Center for Cardiovascular Research (grants FKZ81Z0700107, FKZ 81Z0700108, and FKZ81X2700133), the Fondation Leducq (grant 18CVD02, PlaqOmics) and its Junior Investigator Award (to R. Aherrahrou and T. Reinberger), and the Deutsche Forschungsgemeinschaft (German Research Foundation) under Germany's Excellence Strategy grant EXC 22167-390884018 to HS and as part of the collaborative research centers SFB 1123 (B02 to T. Kessler and H. Schunkert) and TRR 267 (B06 to H. Schunkert). This study was also supported by an American Heart Association Postdoctoral

Fellowship (grant 18POST33990046 to R. Aherrahrou), the National Institutes of Health grant (R21 HL135230 to M. Civelek), the University of Eastern Finland (grant FI22857339 to R. Aherrahrou), and the German Federal Ministry of Education and Research (BMBF) in the context of the DZHK-Säule-B projects (grant FKZ 81X2700121). In addition, this work was supported by the Corona Foundation as part of the Junior Research Group Translational Cardiovascular Genomics (grant S199/10070/2017).

Disclosures

None.

Supplemental Material

Tables S1–S9
Figures S1–S13
Uncropped Western blots
Major Resources Table (Including ARRIVE)

REFERENCES

1. GBD 2016 Causes of Death Collaborators. Global, regional, and national age-sex specific mortality for 264 causes of death, 1980-2016: a systematic analysis for the Global Burden of Disease Study 2016. *Lancet*. 2017;390:1151–1210. doi: 10.1016/S0140-6736(17)32152-9
2. Samani NJ, Erdmann J, Hall AS, Hengstenberg C, Mangino M, Mayer B, Dixon RJ, Meitinger T, Braund P, Wichmann H-E, et al; WTCCC and the Cardiogenics Consortium. Genomewide association analysis of coronary artery disease. *N Engl J Med*. 2007;357:443–453. doi: 10.1056/NEJMoa072366
3. Kathiresan S, Voight BF, Purcell S, Musunuru K, Ardissino D, Mannucci PM, Anand S, Engert JC, Samani NJ, Schunkert H, et al. Genome-wide association of early-onset myocardial infarction with single nucleotide polymorphisms and copy number variants. *Nat Genet*. 2009;4:334–341. doi: 10.1038/ng.327
4. Schunkert H, König IR, Kathiresan S, Reilly MP, Assimes TL, Holm H, Preuss M, Stewart AFR, Barbalic M, Gieger C, et al; Cardiogenics. Large-scale association analysis identifies 13 new susceptibility loci for coronary artery disease. *Nat Genet*. 2011;43:333–338. doi: 10.1038/ng.784
5. Lu X, Wang LL, Chen S, He L, Yang X, Shi Y, Cheng J, Zhang L, Gu CC, Huang J, et al; Coronary ARtery DIsease Genome-Wide Replication And Meta-Analysis (CARDIoGRAM) Consortium. Genome-wide association study in Han Chinese identifies four new susceptibility loci for coronary artery disease. *Nat Genet*. 2012;44:890–894. doi: 10.1038/ng.2337
6. Nikpay M, Goel A, Won H-H, Hall LM, Willenborg C, Kanoni S, Saleheen D, Kyriakou T, Nelson CP, Hopewell JC, et al. A comprehensive 1000 genomes–based genome-wide association meta-analysis of coronary artery disease. *Nat Genet*. 2015;47:1121–1130. doi: 10.1038/ng.3396
7. Jones PD, Kaiser MA, Najafabadi MG, McVey DG, Beveridge AJ, Schofield CL, Samani NJ, Webb TR. The coronary artery disease-associated coding variant in zinc finger C3HC-type containing 1 (ZC3HC1) affects cell cycle regulation. *J Biol Chem*. 2016;291:16318–16327. doi: 10.1074/jbc.M116.734020
8. Ishigaki K, Akiyama M, Kanai M, Takahashi A, Kawakami E, Sugishita H, Sakaue S, Matoba N, Low S-K, Okada Y, et al. Large-scale genome-wide association study in a Japanese population identifies novel susceptibility loci across different diseases. *Nat Genet*. 2020;52:669–679. doi: 10.1038/s41588-020-0640-3
9. Ouyang T, Bai R-Y, Bassermann F, Klitzing C von, Klumpen S, Miething C, Morris SW, Peschel C, Duyster J. Identification and characterization of a Nuclear Interacting Partner of Anaplastic lymphoma kinase (NIPA). *J Biol Chem*. 2003;278:30028–30036. doi: 10.1074/jbc.M300883200
10. Bassermann F, von Klitzing C, Münch S, Bai R-Y, Kawaguchi H, Morris SW, Peschel C, Duyster J. NIPA defines an SCF-type mammalian E3 ligase that regulates mitotic entry. *Cell*. 2005;122:45–57. doi: 10.1016/j.cell.2005.04.034
11. Linseman T, Soubeyrand S, Martinuk A, Nikpay M, Lau P, McPherson R. Functional validation of a common nonsynonymous coding variant in ZC3HC1 associated with protection from coronary artery disease. *Circ Cardiovasc Genet*. 2017;10:e001498. doi: 10.1161/CIRCGENETICS.116.001498
12. van der Harst P, Verweij N. Identification of 64 novel genetic loci provides an expanded view on the genetic architecture of coronary artery disease. *Circ Res*. 2018;122:433–443. doi: 10.1161/CIRCRESAHA.117.312086
13. López-Mejías R, Genre F, García-Bermúdez M, Corrales A, González-Juanatey C, Llorca J, Miranda-Filloy JA, Rueda-Gotor J, Blanco R, Castañeda S, et al. The ZC3HC1 rs11556924 polymorphism is associated with increased carotid intima-media thickness in patients with rheumatoid arthritis. *Arthritis Res Ther*. 2013;15:R152. doi: 10.1186/ar4335
14. ZC3HC1 Gene – GeneCards. 2016. Accessed March 28, 2023. https://www.genecards.org/cgi-bin/carddisp.pl?gene=ZC3HC1&keywords=ZC3HC1
15. Gunkel P, Iino H, Krull S, Cordes VC. ZC3HC1 is a novel inherent component of the nuclear basket, resident in a state of reciprocal dependence with TPR. *Cells*. 2021;10:1937. doi: 10.3390/cells10081937
16. TPR Gene – GeneCards. 2016. Accessed March 28, 2023. https://www.genecards.org/cgi-bin/carddisp.pl?gene=TPR&keywords=TPR
17. Smolock E, Berk BC. *Chapter 98 - vascular smooth muscle cell remodeling in atherosclerosis and restenosis*. Academic Press; 2012:1301–1309.
18. Moser J, van Ark J, van Dijk MC, Greiner DL, Shultz LD, van Goor H, Hillebrands J-L. Distinct differences on neointima formation in immunodeficient and humanized mice after carotid or femoral arterial injury. *Sci Rep*. 2016;6:35387. doi: 10.1038/srep35387
19. Aherrahrou R, Guo L, Nagraj VP, Aguhob A, Hinkle J, Chen L, Yuhl Soh J, Lue D, Alencar GF, Boltjes A, et al. Genetic regulation of atherosclerosis-relevant phenotypes in human vascular smooth muscle cells. *Circ Res*. 2020;127:1552–1565. doi: 10.1161/CIRCRESAHA.120.317415
20. Dobin A, Davis CA, Schlesinger F, Drenkow J, Zaleski C, Jha S, Batut P, Chaisson M, Gingeras TR. STAR: ultrafast universal RNA-seq aligner. *Bioinformatics*. 2013;29:15–21. doi: 10.1093/bioinformatics/bts635
21. DeLuca DS, Levin JZ, Sivachenko A, Fennell T, Nazaire M-D, Williams C, Reich M, Winckler W, Getz G. RNA-SeQC: RNA-seq metrics for quality control and process optimization. *Bioinformatics*. 2012;28:1530–1532. doi: 10.1093/bioinformatics/bts196
22. Liang Y, Aguet F, Barbeira AN, Ardlie K, Im HK. A scalable unified framework of total and allele-specific counts for cis-QTL, fine-mapping, and prediction. *Nat Commun*. 2021;12:1424. doi: 10.1038/s41467-021-21592-8
23. Song G, Lin D, Bao L, Jiang Q, Zhang Y, Zheng H, Gao Q. Effects of high glucose on the expression of LAMA1 and biological behavior of choroid retinal endothelial cells. *J Diabetes Res*. 2018;2018:7504614. doi: 10.1155/2018/7504614
24. Livak KJ, Schmittgen TD. Analysis of relative gene expression data using real-time quantitative PCR and the 2(-Delta Delta C(T)) method. *Methods*. 2001;25:402–408. doi: 10.1006/meth.2001.1262
25. Aherrahrou Z, Doehring LC, Ehlers E-M, Liptau H, Depping R, Linsel-Nitschke P, Kaczmarek PM, Erdmann J, Schunkert H. An alternative splice variant in Abcc6, the gene causing dystrophic calcification, leads to protein deficiency in C3H/He mice. *J Biol Chem*. 2008;283:7608–7615. doi: 10.1074/jbc.M708290200
26. Love MI, Huber W, Anders S. Moderated estimation of fold change and dispersion for RNA-seq data with DESeq2. *Genome Biol*. 2014;15:550. doi: 10.1186/s13059-014-0550-8
27. Franceschini A, Szklarczyk D, Frankild S, Kuhn M, Simonovic M, Roth A, Lin J, Minguez P, Bork P, von Mering C, et al. STRING v9.1: protein-protein interaction networks, with increased coverage and integration. *Nucleic Acids Res*. 2013;41:D808–D815. doi: 10.1093/nar/gks1094
28. Zhou S, Yin X, Mayr M, Noor M, Hylands PJ, Xu Q. Proteomic landscape of TGF-β1-induced fibrogenesis in renal fibroblasts. *Sci Rep*. 2020;10:19054. doi: 10.1038/s41598-020-75989-4
29. Ritchie ME, Phipson B, Wu D, Hu Y, Law CW, Shi W, Smyth GK. limma powers differential expression analyses for RNA-sequencing and microarray studies. *Nucleic Acids Res*. 2015;43:e47. doi: 10.1093/nar/gkv007
30. Kessler T, Zhang L, Liu Z, Yin X, Huang Y, Wang Y, Fu Y, Mayr M, Ge Q, Xu Q, et al. ADAMTS-7 inhibits re-endothelialization of injured arteries and promotes vascular remodeling through cleavage of thrombospondin-1. *Circulation*. 2015;131:1191–1201. doi: 10.1161/CIRCULATIONAHA.114.014072
31. Sata M, Maejima Y, Adachi F, Fukino K, Saiura A, Sugiura S, Aoyagi T, Imai Y, Kurihara H, Kimura K, et al. A mouse model of vascular injury that induces rapid onset of medial cell apoptosis followed by reproducible neointimal hyperplasia. *J Mol Cell Cardiol*. 2000;32:2097–2104. doi: 10.1006/jmcc.2000.1238
32. Wierer M, Werner J, Wobst J, Kastrati A, Cepele G, Aherrahrou R, Sager HB, Erdmann J, Dichgans M, Flockerzi V, et al. A proteomic atlas of the neointima identifies novel druggable targets for preventive therapy. *Eur Heart J*. 2021;42:1773–1785. doi: 10.1093/eurheartj/ehab140
33. Hemani G, Zheng J, Elsworth B, Wade KH, Haberland V, Baird D, Laurin C, Burgess S, Bowden J, Langdon R, et al. The MR-Base platform supports systematic causal inference across the human phenome. *eLife*. 2018;7:e34408. doi: 10.7554/eLife.34408
34. Buniello A, MacArthur JAL, Cerezo M, Harris LW, Hayhurst J, Malangone C, McMahon A, Morales J, Mountjoy E, Sollis E, et al. The NHGRI-EBI GWAS

Catalog of published genome-wide association studies, targeted arrays and summary statistics 2019. *Nucleic Acids Res*. 2019;47:D1005–D1012. doi: 10.1093/nar/gky1120
35. Rotival M, Zeller T, Wild PS, Maouche S, Szymczak S, Schillert A, Castagné R, Deiseroth A, Proust C, Brocheton J, et al; Cardiogenics Consortium. Integrating genome-wide genetic variations and monocyte expression data reveals trans-regulated gene modules in humans. *PLoS Genet*. 2011;7:e1002367. doi: 10.1371/journal.pgen.1002367
36. Erbilgin A, Civelek M, Romanoski CE, Pan C, Hagopian R, Berliner JA, Lusis AJ. Identification of CAD candidate genes in GWAS loci and their expression in vascular cells. *J Lipid Res*. 2013;54:1894–1905. doi: 10.1194/jlr.M037085
37. Yap C, Mieremet A, de Vries CJM, Micha D, de Waard V. Six shades of vascular smooth muscle cells illuminated by KLF4 (Krüppel-like factor 4). *Arterioscler Thromb Vasc Biol*. 2021;41:2693–2707. doi: 10.1161/ATVBAHA.121.316600
38. Kuleshov MV, Jones MR, Rouillard AD, Fernandez NF, Duan Q, Wang Z, Koplev S, Jenkins SL, Jagodnik KM, Lachmann A, et al. Enrichr: a comprehensive gene set enrichment analysis web server 2016 update. *Nucleic Acids Res*. 2016;44:W90–W97. doi: 10.1093/nar/gkw377
39. Güttinger S, Laurell E, Kutay U. Orchestrating nuclear envelope disassembly and reassembly during mitosis. *Nat Rev Mol Cell Biol*. 2009;10:178–191. doi: 10.1038/nrm2641
40. Linder MI, Köhler M, Boersema P, Weberruss M, Wandke C, Marino J, Ashiono C, Picotti P, Antonin W, Kutay U. Mitotic disassembly of nuclear pore complexes involves CDK1- and PLK1-mediated phosphorylation of key interconnecting nucleoporins. *Dev Cell*. 2017;43:141–156.e7. doi: 10.1016/j.devcel.2017.08.020
41. Jeong S, Ahn J, Jo I, Kang S-M, Park B-J, Cho H-S, Kim Y-H, Ha N-C. Cyclin-dependent kinase 1 depolymerizes nuclear lamin filaments by disrupting the head-to-tail interaction of the lamin central rod domain. *J Biol Chem*. 2022;298:102256. doi: 10.1016/j.jbc.2022.102256
42. Jackman M, Lindon C, Nigg EA, Pines J. Active cyclin B1–Cdk1 first appears on centrosomes in prophase. *Nat Cell Biol*. 2003;5:143–148. doi: 10.1038/ncb918
43. Hayward D, Alfonso-Pérez T, Gruneberg U. Orchestration of the spindle assembly checkpoint by CDK1-cyclin B1. *FEBS Lett*. 2019;593:2889–2907. doi: 10.1002/1873-3468.13591
44. Kim H, Johnson JM, Lera RF, Brahma S, Burkard ME. Anillin phosphorylation controls timely membrane association and successful cytokinesis. *PLoS Genet*. 2017;13:e1006511. doi: 10.1371/journal.pgen.1006511
45. Chi Y-H, Chen Z-J, Jeang K-T. The nuclear envelopathies and human diseases. *J Biomed Sci*. 2009;16:96. doi: 10.1186/1423-0127-16-96
46. Porter LA, Donoghue DJ. Cyclin B1 and CDK1: nuclear localization and upstream regulators. *Prog Cell Cycle Res*. 2003;5:335–347.
47. Welt FGP, Rogers C. Inflammation and restenosis in the stent era. *Arterioscler Thromb Vasc Biol*. 2002;22:1769–1776. doi: 10.1161/01.atv.0000037100.44766.5b
48. Kim MS, Dean LS. In-stent restenosis. *Cardiovasc Ther*. 2011;29:190–198. doi: 10.1111/j.1755-5922.2010.00155.x
49. Grootaert MOJ, Bennett MR. Vascular smooth muscle cells in atherosclerosis: time for a re-assessment. *Cardiovasc Res*. 2021;117:2326–2339. doi: 10.1093/cvr/cvab046
50. Sorokin V, Vickneson K, Kofidis T, Woo CC, Lin XY, Foo R, Shanahan CM. Role of vascular smooth muscle cell plasticity and interactions in vessel wall inflammation. *Front Immunol*. 2020;11:599415. doi: 10.3389/fimmu.2020.599415
51. Goikuria H, Freijo MM, Manrique RV, Sastre M, Elizagaray E, Lorenzo A, Vandenbroeck K, Alloza I. Characterization of carotid smooth muscle cells during phenotypic transition. *Cells*. 2018;7:23. doi: 10.3390/cells703002
52. Brænne I, Civelek M, Vilne B, Di Narzo A, Johnson AD, Zhao Y, Reiz B, Codoni V, Webb TR, Foroughi Asl H, et al; Leducq Consortium CAD Genomics. Prediction of causal candidate genes in coronary artery disease loci. *Arterioscler Thromb Vasc Biol*. 2015;35:2207–2217. doi: 10.1161/ATVBAHA.115.306108
53. Farb A, Weber DK, Kolodgie FD, Burke AP, Virmani R. Morphological predictors of restenosis after coronary stenting in humans. *Circulation*. 2002;105:2974–2980. doi: 10.1161/01.cir.0000019071.72887.bd
54. Buccheri D, Piraino D, Andolina G, Cortese B. Understanding and managing in-stent restenosis: a review of clinical data, from pathogenesis to treatment. *J Thorac Dis*. 2016;8:E1150–E1162. doi: 10.21037/jtd.2016.10.93
55. Sandison ME, Dempster J, McCarron JG. The transition of smooth muscle cells from a contractile to a migratory, phagocytic phenotype: direct demonstration of phenotypic modulation. *J Physiol*. 2016;594:6189–6209. doi: 10.1113/JP272729
56. Allahverdian S, Chaabane C, Boukais K, Francis GA, Bochaton-Piallat M-L. Smooth muscle cell fate and plasticity in atherosclerosis. *Cardiovasc Res*. 2018;114:540–550. doi: 10.1093/cvr/cvy022
57. Bennett MR, Sinha S, Owens GK. Vascular smooth muscle cells in atherosclerosis. *Circ Res*. 2016;118:692–702. doi: 10.1161/CIRCRESAHA.115.306361
58. Andrés V, Castro C. Antiproliferative strategies for the treatment of vascular proliferative disease. *Curr Vasc Pharmacol*. 2003;1:85–98. doi: 10.2174/1570161033386763
59. O'Brien ER, Alpers CE, Stewart DK, Ferguson M, Tran N, Gordon D, Benditt EP, Hinohara T, Simpson JB, Schwartz SM. Proliferation in primary and restenotic coronary atherectomy tissue. Implications for antiproliferative therapy. *Circ Res*. 1993;73:223–231. doi: 10.1161/01.res.73.2.223
60. Hajar R. Risk factors for coronary artery disease: historical perspectives. *Heart Views*. 2017;18:109–114. doi: 10.4103/HEARTVIEWS.HEARTVIEWS_106_17
61. Khera AV, Kathiresan S. Genetics of coronary artery disease: discovery, biology and clinical translation. *Nat Rev Genet*. 2017;18:331–344. doi: 10.1038/nrg.2016.160
62. Traeuble K, Munz M, Pauli J, Sachs N, Vafadarnejad E, Carrillo-Roa T, Maegdefessel L, Kastner P, Heinig M. Integrated single-cell atlas of human atherosclerotic plaques. *Nat Commun*. 2025;16:8255. doi: 10.1038/s41467-025-63202-x
63. Crnkovic S, Valzano F, Fließer E, Gindlhuber J, Thekkekara Puthenparampil H, Basil M, Morley MP, Katzen J, Gschwandtner E, Klepetko W, et al. Single-cell transcriptomics reveals skewed cellular communication and phenotypic shift in pulmonary artery remodeling. *JCI Insight*. 3471;7:e15. doi: 10.1172/jci.insight.153471
64. Fourest-Lieuvin A, Peris L, Gache V, Garcia-Saez I, Juillan-Binard C, Lantez V, Job D. Microtubule regulation in mitosis: tubulin phosphorylation by the cyclin-dependent kinase Cdk1. *Mol Biol Cell*. 2006;17:1041–1050. doi: 10.1091/mbc.e05-07-0621
65. Singh D, Schmidt N, Müller F, Bange T, Bird AW. Destabilization of long astral microtubules via Cdk1-dependent removal of GTSE1 from their plus ends facilitates prometaphase spindle orientation. *Curr Biol*. 2021;31:766–781.e8. doi: 10.1016/j.cub.2020.11.040
66. Liu J, Fairn GD, Ceccarelli DF, Sicheri F, Wilde A. Cleavage furrow organization requires PIP2-mediated recruitment of anillin. *Curr Biol*. 2012;22:64–69. doi: 10.1016/j.cub.2011.11.040